Ancient plant DNA reveals High Arctic greening during the Last Interglacial

Sarah E. Crump[a,b,1], Bianca Fréchette[c], Matthew Power[d], Sam Cutler[b], Gregory de Wet[a,e], Martha K. Raynolds[f], Jonathan H. Raberg[a], Jason P. Briner[g], Elizabeth K. Thomas[g], Julio Sepúlveda[a], Beth Shapiro[b,h], Michael Bunce[d,i], and Gifford H. Miller[a]

[a]Institute of Arctic and Alpine Research and Department of Geological Sciences, University of Colorado, Boulder, CO 80303; [b]Department of Ecology and Evolutionary Biology, University of California, Santa Cruz, CA 95064; [c]Geotop, Université du Québec à Montréal, Montréal, H2L 2C4, Canada; [d]Trace and Environmental DNA Laboratory, School of Molecular and Life Sciences, Curtin University, 6845 Bentley, Australia; [e]Department of Geosciences, Smith College, Northampton, MA 01063; [f]Institute of Arctic Biology, University of Alaska Fairbanks, Fairbanks, AK 99775; [g]Department of Geology, University at Buffalo, Buffalo, NY 14260; [h]HHMI, University of California, Santa Cruz, CA 95064; and [i]New Zealand Environment Protection Authority, 6011 Wellington, New Zealand

Edited by Cathy Whitlock, Montana State University, Bozeman, MT, and approved February 2, 2021 (received for review September 9, 2020)

Summer warming is driving a greening trend across the Arctic, with the potential for large-scale amplification of climate change due to vegetation-related feedbacks [Pearson et al., *Nat. Clim. Chang.* (3), 673–677 (2013)]. Because observational records are sparse and temporally limited, past episodes of Arctic warming can help elucidate the magnitude of vegetation response to temperature change. The Last Interglacial ([LIG], 129,000 to 116,000 y ago) was the most recent episode of Arctic warming on par with predicted 21st century temperature change [Otto-Bliesner et al., *Philos. Trans. A Math. Phys. Eng. Sci.* (371), 20130097 (2013) and Post et al., *Sci. Adv*. (5), eaaw9883 (2019)]. However, high-latitude terrestrial records from this period are rare, so LIG vegetation distributions are incompletely known. Pollen-based vegetation reconstructions can be biased by long-distance pollen transport, further obscuring the paleoenvironmental record. Here, we present a LIG vegetation record based on ancient DNA in lake sediment and compare it with fossil pollen. Comprehensive plant community reconstructions through the last and current interglacial (the Holocene) on Baffin Island, Arctic Canada, reveal coherent climate-driven community shifts across both interglacials. Peak LIG warmth featured a ∼400-km northward range shift of dwarf birch, a key woody shrub that is again expanding northward. Greening of the High Arctic—documented here by multiple proxies—likely represented a strong positive feedback on high-latitude LIG warming. Authenticated ancient DNA from this lake sediment also extends the useful preservation window for the technique and highlights the utility of combining traditional and molecular approaches for gleaning paleoenvironmental insights to better anticipate a warmer future.

paleoecology | Arctic greening | sedimentary ancient DNA | Last Interglacial

The Arctic is greening as shrub biomass increases and vegetation ranges shift north in response to summer warming (1, 2). This process—one of the clearest terrestrial manifestations of climate change thus far—has major implications both for local ecosystems and for global energy balance and biogeochemical systems (3–5). In particular, taller shrubs darken otherwise snow-covered surfaces, contributing to the albedo feedback (6, 7), and enhanced evapotranspiration is expected to result in a positive greenhouse feedback (8). Shrub cover also impacts soil thermal regime, which may impact permafrost vulnerability (9–11). Because feedbacks related to Arctic greening are complex and potentially large in magnitude, estimating the extent and rate of northward shrub migration is a vital component of predicting future warming.

Past warm periods serve as valuable analogs for understanding the extent of Arctic greening under well-constrained climate conditions. The Last Interglacial (LIG; Marine Isotope Stage [MIS] 5e, 129 to 116 ka [thousands of years before present]) was ∼1 °C warmer than the preindustrial period globally, but the Arctic experienced amplified warming due to higher summer insolation anomalies and positive feedbacks at high latitudes (12, 13). The Eastern Canadian Arctic and Greenland, in particular, were likely ∼4 to 8 °C warmer in summer than present (Fig. 1) (14–18). LIG sediment records from this region thus provide an archive of the vegetation response to Arctic warming at levels comparable to predicted 21st-century climate change (19).

While most High Arctic lake basins were scraped clean by ice sheet erosion during the last glaciation and thus only contain postglacial sediments, lakes with small, low-relief catchments within regions of cold-based, slow-flowing ice were protected from erosion. Several such sites have been discovered on eastern Baffin Island, Arctic Canada and contain stratified records of multiple interglacials (20–22). Previous work from Lake CF8 on northeastern Baffin Island (Fig. 1 and *SI Appendix*, Fig. S1) demonstrates that its sediment record spans at least three interglacials (∼200 ka), including a substantially warmer-than-present LIG as indicated by chironomids, diatoms, and geochemical proxies (15, 23).

Significance

The Arctic is warming exceptionally rapidly, promoting an expansion of shrubs across the Arctic with global-scale climate implications. The Last Interglacial (∼125,000 y ago) was the most recent time the Arctic was warmer than present and thus serves as an analogue for Arctic greening in the near future. Ancient plant DNA in lake sediment from this time reveals major ecosystem changes in response to warmth, including an ∼400 km northward shift of dwarf birch relative to today. Enhanced shrub cover, corroborated by molecular and microfossil analyses, amplified warming during the Last Interglacial and will likely play a similar role in the future. This record constitutes the oldest authenticated plant DNA from lake sediment yet reported, increasing the technique's temporal potential.

Author contributions: S.E.C., B.S., M.B., and G.H.M. designed research; S.E.C., B.F., M.P., S.C., G.d.W., M.K.R., J.H.R., J.P.B., E.K.T., and J.S. performed research; S.E.C., B.F., S.C., G.d.W., M.K.R., and J.P.B. analyzed data; G.d.W., M.K.R., J.H.R., J.P.B., E.K.T., and J.S. helped with interpretation of data; B.S., M.B., and G.H.M. supervised the research and helped with interpretation of data; and S.E.C. wrote the paper with input from all coauthors.

The authors declare no competing interest.

This article is a PNAS Direct Submission.

[1]To whom correspondence may be addressed. Email: sarah.crump@colorado.edu.

This article contains supporting information online at https://www.pnas.org/lookup/suppl/doi:10.1073/pnas.2019069118/-/DCSupplemental.

Published March 15, 2021.

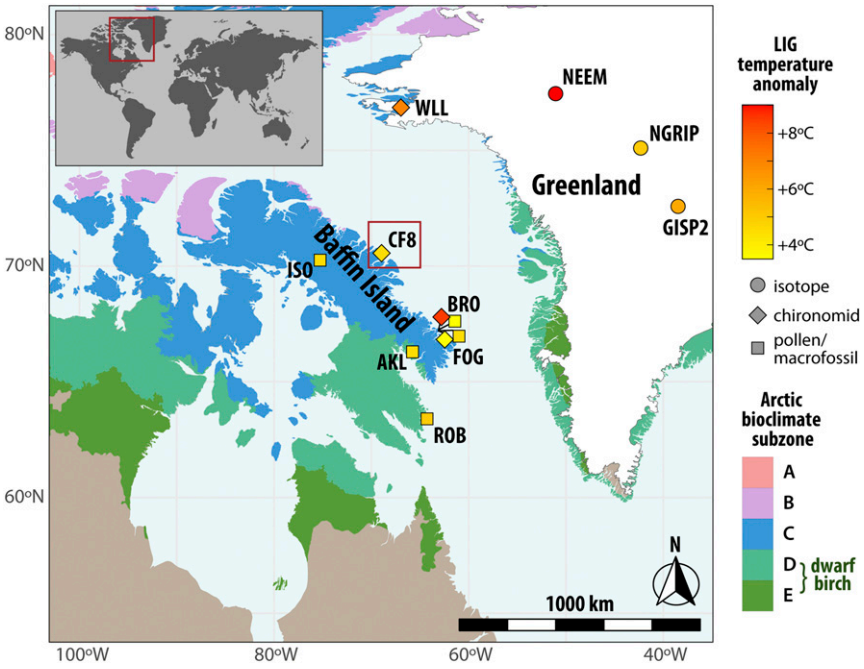

Fig. 1. Map of Baffin Island and Lake CF8 study area. The symbols represent maximum LIG temperature anomalies based on terrestrial proxy records (shape indicates proxy type) from Baffin Island and Greenland (see *SI Appendix*, Table S1 for metadata). The shaded regions indicate Arctic bioclimate subzones delineations (29), including modern *Betula* range in subzones D and E. We note that a small outlier population of *Betula* occurs east of the D/E boundary on Baffin Island (not captured by vegetation map resolution) (38).

We targeted the multi-interglacial record from Lake CF8 to assess the vegetation response to pronounced warmth during the LIG and moderate warmth during the Holocene. Pollen produced by some key shrubs and trees, including *Betula* (birch), is efficiently wind-transported and thus present in lake sediments far north of their ranges (24, 25). We therefore analyzed both sedimentary ancient DNA (sedaDNA), which is sourced locally from within the lake catchment and does not include pollen-derived DNA (26), and fossil pollen to generate a robust vegetation record spanning the last ∼130 ka. Taken together, DNA-inferred plant communities and pollen-inferred July air temperatures provide insight into Arctic plant range shifts under strong summer warming.

Results

Lake CF8 (70.55818°N, 68.94968°W) is a small lake (surface area = 0.05 km^2, max depth = ∼10 m; *SI Appendix*, Fig. S1) situated at 195 m above sea level on the Clyde Foreland, a broad coastal lowland of northeastern Baffin Island (Fig. 1). Its small catchment (∼0.2 km^2) is typical of a High Arctic tundra (27, 28) or Arctic Bioclimate Subzone C (29). The modern plant communities include dry crustose and foliose lichens on rocks; wet graminoid and bryophyte communities on sorted-stripe slopes; and moist prostrate dwarf-shrub, sedge, and bryophyte communities on sorted polygons. Prostrate dwarf willows (*Salix spp.*) are rare (*SI Appendix*, Fig. S2). The upper slopes of the catchment feature frost-riven boulders, while glacial-fluvial sorting has deposited gravel and finer materials closer to the lake. Frost sorting has created stripes and polygons of finer materials that support the majority of soil development and vegetation cover.

The CF8 sediment record is dominated by three organic-rich lacustrine sediment units that represent interglacial periods separated by sandy units that likely represent the waning stages of glacial periods following extensive depositional hiatuses (Fig. 2) (15, 20). The stratigraphy of cores collected in 2017 and 2019 correlate well with previously studied cores from CF8, lending confidence to interglacial assignments based on published age controls (*SI Appendix*, Fig. S3). In all cores, radiocarbon ages from plant macrofossils below the Holocene unit are >40 ^{14}C ka, indicating those units are beyond the radiocarbon dating window (Fig. 2 and *SI Appendix*, Table S2). The lowest interglacial unit in previously published cores yielded an optically stimulated luminescence (OSL) date of >194 ka and is thus assigned to the Penultimate Interglacial (PIG), MIS 7 (20). The next youngest interglacial is bounded by OSL dates of ∼122 and ∼100 ka (Fig. 2). Based on these dates and the lithostratigraphy of the core, we interpret this interval to represent the LIG but refrain from assigning absolute ages within the unit due to the large uncertainties (≥10 ka) associated with OSL dating. A thin nonglacial unit between the LIG and Holocene units is tentatively assigned to interstadial MIS 5a based on ^{14}C dates >45 ka and the timing of maximum summer insolation across the Arctic (20, 30). We developed an age–depth model for the Holocene (12 ka to present) based on eight radiocarbon ages on plant macrofossils (*SI Appendix*, Fig. S4 and Table S2). Hereafter, we primarily focus on the LIG and Holocene units, where plant DNA preservation is adequate and interglacial assignment is most secure.

We extracted and analyzed sedaDNA from the 2017 (Holocene) and 2019 (pre-Holocene) CF8 cores in dedicated ancient DNA facilities at Curtin University, Australia (see *Materials and Methods*). Targeting the P6 loop of the chloroplast trnL (UAA) intron (31), we amplified vascular plant DNA via PCR and sequenced the resulting amplicons following a standard metabarcoding approach (32). In the Holocene core, 41 of 46 samples passed our final quality filter (Fig. 2 and see *Materials and Methods*), indicating sufficient yields of endogenous plant DNA in 89% of analyzed levels. Following filtering, Holocene samples averaged 43,651 reads and 5.7 ± 2.8 (mean ±1 SD) taxa per sample, with no clear decrease in preservation over the last 12 ka (*SI Appendix*, Fig. S5). In the LIG core, 42 of 58 samples (72%) passed the final filter. Samples averaged 7,671 reads and 2.8 ± 1.0 taxa

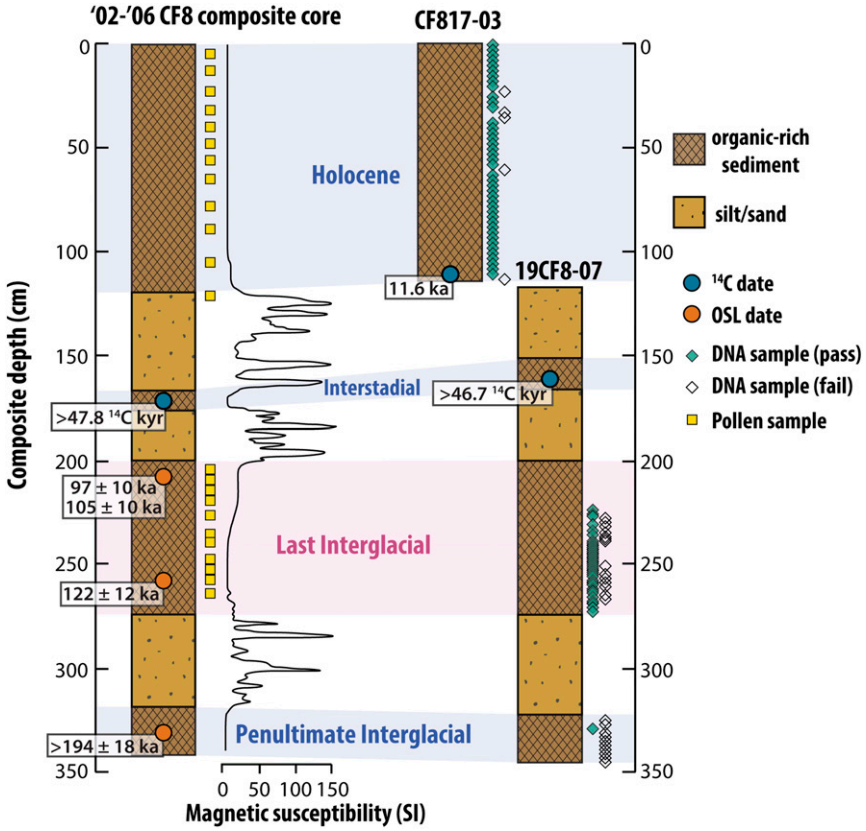

Fig. 2. Lake CF8 core lithostratigraphy and sampling summary. Core diagrams show simplified sediment character and interglacial/interstadial assignments for previously published CF8 cores (2002 to 2006) (20, 23, 84) and new (2017 and 2019) CF8 cores. Magnetic susceptibility for 2002 to 2006 cores shows contrast between organic-rich (interglacial) units and minerogenic (deglacial) units. The key age control points (*SI Appendix*, Table S2) and pollen and DNA sample depths are shown with symbols defined in the legend.

(*SI Appendix*, Fig. S5). Reduced yields and lower per-sample plant diversity in the LIG unit is an expected result of the >100-kyr age difference between LIG and Holocene samples, as DNA damage is known to accumulate through time in lake sediments (33). Of 30 total plant taxa identified, 12 are common to both interglacials, with 5 unique to the LIG and 13 occurring only in the Holocene (*SI Appendix*, Tables S3 and S4 and Fig. S2). Downcore trends in the dominant taxa (those occurring as >1% of reads in ≥2 samples) are summarized in Fig. 3. Pilot samples from the PIG largely failed to yield amplifiable DNA; only 1 of 12 samples passed final quality filtering, and it contained only one taxon (Salicaceae) (*SI Appendix*, Table S3). We thus consider the >190-ka unit from this site to be beyond the useful preservation window for the extraction and metabarcoding techniques employed here.

To verify the authenticity of the plant DNA within the LIG unit, we conducted shotgun sequencing on a subset of samples (see *Materials and Methods* and *SI Appendix*), one from the early Holocene (9.5 ka) and two from the LIG (at 242.5- and 246.5-cm depths). We investigated nucleotide misincorporation patterns by aligning each library to available complete plant reference genomes. For the two samples (both LIG) with a sufficient number of aligned reads aligned to the *Salix brachista* genome, we observed the increased rate of C to T (G to A) transitions at read starts (stops) known to characterize bona fide ancient DNA templates (*SI Appendix*, Figs. S6 and S7). These aligned reads were also short, with the LIG samples averaging 44 ± 11 base pairs (bp) in length (median ±1 SD) (*SI Appendix*, Figs. S8–S10).

We analyzed fossil pollen in sediment samples from previously published CF8 cores and aligned with the sedaDNA record using age–depth models (Holocene; *SI Appendix*, Fig. S4) and bulk geochemical trends (LIG; see *SI Appendix*, text and Fig. S3). Holocene sediments are dominated by pollen from herbs and heaths, while LIG sediments contain larger proportions of shrub taxa, including *Betula* (Fig. 3 and *SI Appendix*, Fig. S11 and Table S5). Pollen concentrations are on average higher in the LIG (72,600 grains per g dry sediment) compared to the Holocene (19,600 grains per g dry sediment) (Fig. 4 and *SI Appendix*, Table S5). We note that while concentrations in grains per gram of dry sediment account for differences in density between the two units, we cannot compare pollen fluxes because of a lack of age control within the LIG. An increase in pollen concentration in the late LIG is likely related to a reduction in background sedimentation rate rather than an increase in pollen flux. July air temperatures inferred from pollen assemblages (using the modern analog technique; see *Materials and Methods*) are highest in the LIG and ranged from ~4 to 8 °C (Fig. 3).

Discussion

Plant Community Changes across Interglacials. The Holocene and LIG units contain genetic evidence for similar millennial-scale patterns of vegetation change, despite differences in peak plant communities. Constrained hierarchical clustering analysis resulted in the division of each interglacial into three biostratigraphic units based on the sedaDNA results (Fig. 3 and *SI Appendix*, Fig. S12) (34, 35). The distinct plant communities of the three units follow a broadly consistent interglacial pattern: 1) warming out

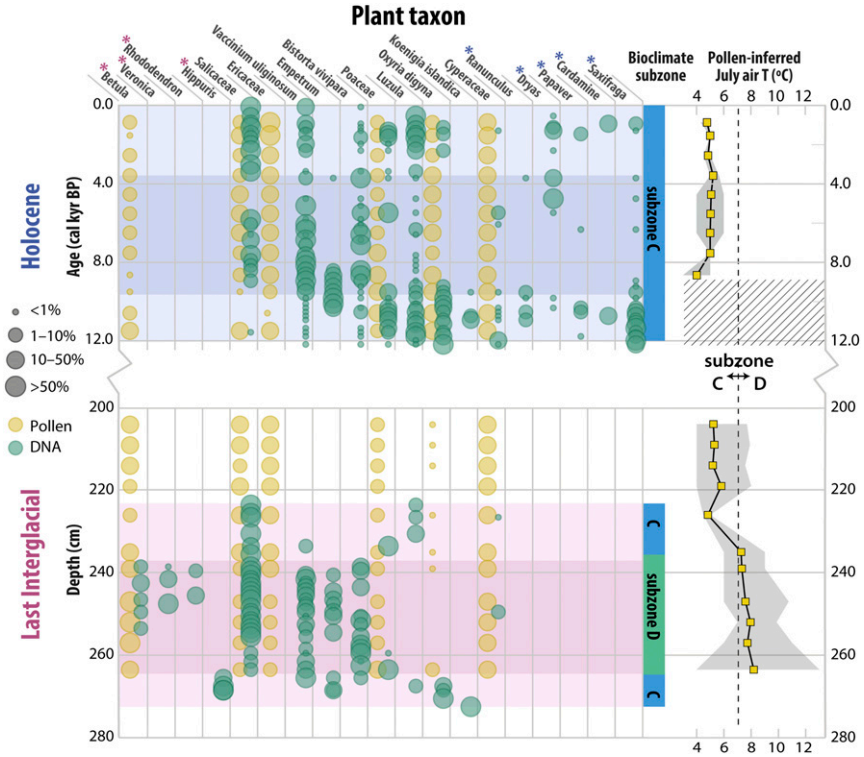

Fig. 3. Vegetation and climate history at Lake CF8. Results from DNA metabarcoding (green circles; taxa occurring as >1% of reads in ≥2 samples included) and pollen (yellow circles; taxa averaging >5% included) are shown as circles scaled to relative abundance of sample reads or pollen grains (grouped into four percentage bins shown in legend). Note that in the LIG, no DNA analyses were completed above 223.5 cm, and no pollen analyses were completed below 263.5 cm. The pink and blue shading delineates biostratigraphic units (lower, middle, and upper for each interglacial) inferred from constrained hierarchical clustering of sedaDNA metabarcoding results. The pink and blue asterisks indicate taxa only occurring in the LIG and the Holocene, respectively, based on sedaDNA. Bioclimate subzone assignment (colors correspond to Fig. 1) is based on sedaDNA-inferred taxa presence within each unit. Pollen-inferred July air temperature estimate is based on the modern analog technique and includes the temperature range (gray band) from the five best modern analogs (see *Materials and Methods*). The dashed line indicates mean July temperature threshold (7 °C) defining the boundary between subzones C and D. The hatched area denotes interval with no adequate modern analog. Note the break in the *y*-axis and that Holocene samples are plotted on age scale while LIG samples are plotted on depth scale.

of the glacial and early colonization of the landscape; 2) peak vegetation following peak summer warmth driven by high summer insolation; and 3) a shift back toward cold-tolerant taxa as summers cooled due to decreasing summer insolation. This consistent interglacial temporal pattern is captured by nonmetric multidimensional scaling ordination analysis (*SI Appendix*, Fig. S13) and is described below.

The lowest unit in both interglacials is characterized by early colonizers and/or cold-tolerant taxa, including *Koenigia islandica*, *Oxyria digyna*, and *Luzula*. The early Holocene also featured the relatively hardy taxa *Saxifraga*, *Ranunculus*, *Papaver*, and *Carex*, while the early LIG also featured the aquatic plant *Hippuris.* While the presence of *Hippuris*—which favors shallow water habitats (36)—could indicate a decrease in lake level during the early LIG, the current lake geometry includes some favorable shallow settings, and so a lake level change is not required.

Subsequently, a similar pattern of woody shrub establishment is apparent moving into the middle unit of both interglacials: High levels (>10%) of *Empetrum* occur first, followed by *Vaccinium uliginosum*, and then Salicaceae [(likely *Salix spp* (36)]. In the Holocene, Salicaceae is not consistently present until ∼8.9 ka, which was >3 ka after the catchment deglaciated. While absolute age control is unavailable for the LIG, a migration lag is apparent in the absence of Salicaceae from the lowest ∼10 cm (∼14%) of the interglacial unit. *Betula* [likely *B. glandulosa* or *B. nana*, dwarf birch (36)] is absent in the Holocene unit but appears in the LIG and remains present through much of its middle biostratigraphic unit. This result is consistent with warmer peak temperatures in the LIG than the Holocene, favoring northward migration of this subarctic shrub (17). The average pollen-inferred July temperature for the LIG middle unit is 8 °C (range: 6 to 11 °C), which is ∼3 °C above the modern mean July air temperature (*SI Appendix*) and the pollen-inferred Holocene average (5 °C) (Fig. 3). The absence of *Betula* DNA in the lowest ∼20 cm (∼27%) of the LIG despite favorable pollen-inferred temperatures suggests a pronounced migration lag—in concordance with the postglacial migration lag evident in a Holocene sedaDNA record from a southern Baffin Island lake core (32).

The upper unit of both interglacials is characterized by a shift back to relatively cold-tolerant taxa. This pattern is an expected manifestation of decreasing summer insolation through the interglacials (30), resulting in cooler summers—captured by a sharp decrease in pollen-inferred temperatures in the upper LIG unit and modest cooling in the late Holocene (Fig. 3). *Betula* disappears in the late LIG, and *Empetrum* is absent in the upper unit of both interglacials. The reappearance/expansion of *Luzula* and Poaceae occurs late in both interglacials. *Saxifraga* and *Dryas* also characterize the cooler late Holocene but have disappeared from the modern flora (*SI Appendix*, Fig. S2).

We note that while the pollen record largely corroborates the plant community at Lake CF8 through time, it indicates a less dynamic vegetation history than that inferred from sedaDNA (*SI Appendix*, Fig. S11). We suggest that this is due to reduced taxonomic resolution for some taxa and because pollen captures a

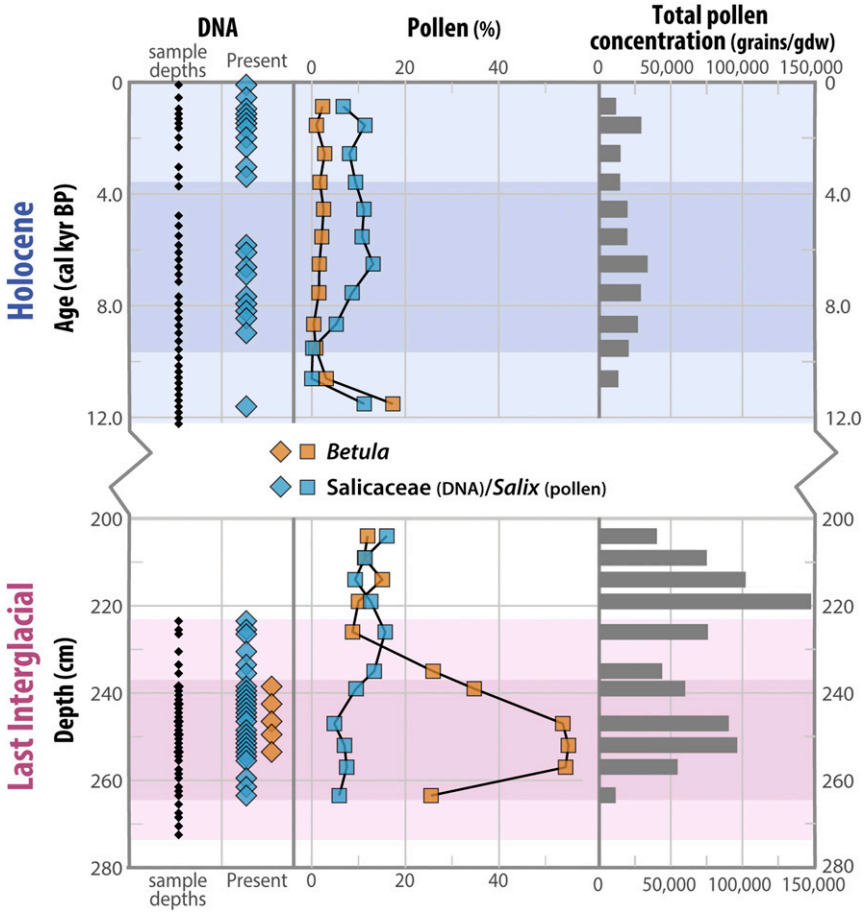

Fig. 4. Multiproxy evidence for local *Betula* presence. The downcore trends for dominant woody shrubs *Betula* and Salicaceae (assumed *Salix*) based on DNA metabarcoding (diamonds; as presence) and pollen (squares; as percent of total pollen grains). Total pollen concentration (grains per g dry weight of sediment) highlights enhanced biomass in the LIG versus Holocene. The pink and blue shading delineates biostratigraphic units as in Fig. 3. Note the break in the *y*-axis and that Holocene samples are plotted on age scale while LIG samples are plotted on depth scale.

more regional vegetation signal than sedaDNA (25, 37), including low to modest levels of wind-transported pollen from boreal trees, *Alnus*, and *Betula* when they were likely not growing near Lake CF8. Early in the interglacials following deglaciation, pollen may be sourced in part from older deposits on the landscape, whereas sedaDNA is unlikely to be preserved in reworked soils. We thus expect sedaDNA to more closely reflect local plant presence (and therefore timing of establishment/extirpation), whereas the pollen record represents a regionally smoothed vegetation history (25). Combining the two vegetation proxies—particularly given the greater preservation potential of pollen—enables a more robust approach to assessing ecosystem changes over the two interglacials compared to using either proxy alone.

Last Interglacial Shrub Range Shifts. The DNA metabarcoding results provide compelling evidence that dwarf birch, a relatively cold-intolerant woody shrub that typifies the Low Arctic tundra and whose northern limit is currently ∼400 km south in the Eastern Canadian Arctic (38) (Fig. 1), was present at Lake CF8 during the LIG. *Betula* DNA was identified in five levels within the middle LIG unit, and it was not present (even prior to quality filtering) in any extraction controls or in any of the 46 Holocene samples (Fig. 3 and *SI Appendix*, Tables S3 and S4). *Betula* co-occurs with two other taxa, *Veronica* and *Rhododendron*, that were not present at CF8 during the Holocene. *Veronica* is currently found only at warmer, more southerly sites in the Eastern Canadian Arctic (36), while *Rhododendron* has been observed in Bioclimate Subzone C but is currently absent from the Clyde Foreland region. The interval with these three taxa defines the peak vegetation community at CF8 and is characteristic of Bioclimate Subzone D, which has a mean July temperature range of 7 to 9 °C (2 to 4 °C warmer than present; see *SI Appendix*) (29). This shift is consistent with peak LIG warmth of ∼3 °C above the late 20th century inferred from pollen (Fig. 3) and 4 to 5 °C above the late 20th century inferred from chironomid assemblages at CF8 (15) (Fig. 1).

A northward shift in the dwarf birch range is corroborated by a pronounced increase in *Betula* pollen during the middle LIG unit in CF8 sediment (Fig. 4). While low amounts of wind-transported *Betula* pollen are present throughout the CF8 Holocene record (<4% over the last 11 ka), the LIG sediment interval with DNA-inferred peak vegetation contains 25 to 55% *Betula* pollen. This peak in *Betula* pollen is consistent with local dwarf birch presence and an ∼400 km northward shift of Bioclimate Subzone D on Baffin Island. The average total pollen concentration for the LIG is nearly fourfold higher than the Holocene, further supporting an Arctic greening signal.

A northward migration of shrubs during the LIG has been inferred from other paleobotanical records from Baffin Island and elsewhere in the Arctic. A buried LIG soil section ∼20 km east of CF8 contains >50% *Betula* pollen, consistent with its local presence in the area (39). Pollen records from three lakes on southern Baffin Island (FOG, BRO, and AKL in Fig. 1) indicate a shrub tundra during the LIG, including the local establishment

of *Betula* and possibly *Alnus* (alder) outside of their current limits, but range shift magnitudes are unclear due to the regional sourcing of pollen (17). Pollen in marine sediment southwest of Greenland also suggest enhanced shrub (alder and birch) cover on Greenland in the LIG compared to the Holocene (40). Moreover, substantial northward shifts of boreal treeline have been documented in paleorecords from northwest Alaska (41) and Siberia (42, 43). Widespread poleward range expansions during the LIG highlight important feedbacks between the climate system and biosphere during past warm periods.

Paleoclimate models have largely underestimated the magnitude of Arctic warming during the LIG (12, 44), and this discrepancy with proxy data may be related to models inadequately capturing vegetation-related feedbacks. Summer insolation at high northern latitudes during the early LIG was exceptionally high (45), with peak insolation at 127 ka occurring after sea level reached modern levels (46). This suggests that unlike during the Holocene, the penultimate continental ice sheets had largely disappeared prior to the insolation maximum of the LIG, enabling excess solar radiation to drive strong terrestrial warming (sensible heat) rather than ice ablation (latent heat). Thus, high-latitude landscapes were ice-free in time for more significant vegetation shifts compared to the Holocene. Models assessing LIG climate dynamics have identified vegetation changes, and especially the interplay between vegetation and snow cover (i.e., taller vegetation masking the high albedo of seasonal snow), as the most critical feedback amplifying high-latitude warming (47), including a near doubling of high-latitude temperature changes (48). Emerging climate model evidence suggests that Arctic vegetation feedbacks also play a large role in determining Greenland Ice Sheet mass balance and thus its contribution to sea level rise (49, 50). Such findings underscore the need for more spatially precise vegetation records from the LIG, especially as near-future climate change may be similarly amplified by as-yet unconstrained Arctic greening.

DNA Preservation in >100 ka Lake Sediment. The Lake CF8 sediment record presents a valuable opportunity to assess the preservation potential of sedaDNA in favorable (cool) settings. Our DNA metabarcoding results indicate a systematic reduction in DNA preservation through progressively older interglacials (Fig. 2 and *SI Appendix*, Fig. S5), but sediment between ∼100 and 130 ka contains sufficiently well-preserved DNA for amplifying a 30- to 85-bp region of chloroplast DNA. This extends substantially the useful timeframe for authenticated lake sediment–based ancient DNA studies, which have so far focused on latest Pleistocene (<30 ka) and Holocene timescales (26, 51). We demonstrate through multiple lines of evidence that the LIG DNA is indeed endogenous and can provide ecologically meaningful information. The plant taxa inferred from sedimentary DNA within the CF8 LIG unit align well with ecological and paleoclimatic predictions, are replicable within the core, and are bioinformatically robust (see *SI Appendix*). Shotgun sequencing of LIG DNA extracts reveals clear damage patterns (nucleotide misincorporation and short fragment lengths) that confirm their ancient origin (*SI Appendix*, Figs. S6–S10).

As the greening of the Arctic proceeds due to human-caused climate change, precise and detailed paleoecological records from past warm periods are essential to anticipate the extent of future greening. Evidence for shrub range shifts in >100-ka sedimentary DNA underscore the potential to generate more taxonomically resolved, location-specific paleovegetation records from past interglacials than has been possible with traditional proxies alone. Given the potentially strong vegetation-related climate feedbacks initiated by northward shrub expansion, LIG sedaDNA records may elucidate the nature of environmental changes through warmer-than-present conditions and thereby help to improve the predictive power of climate models.

Materials and Methods

Core Collection, Description, and Age Control. The Holocene sediment core (CF817-03) was collected in August 2017 using a Bolivia-type corer from an inflatable raft. The pre-Holocene sediment core (19CF8-07) was collected in May 2019 using a modified Nesje corer and aluminum core tube from the frozen lake surface. Both cores were taken from the central deep basin of the lake (*SI Appendix*, Fig. S1). Cores were transferred to cold room (4° C) storage prior to splitting and sampling within 9 mo of collection. Cores were split at the Trace and Environmental DNA (TrEnD) Lab at Curtin University (CF817-03) and the Sedimentology Lab at University of Colorado Boulder (19CF8-07) using bleach-cleaned tools and described immediately to note visual transitions between units.

A Holocene age–depth model was developed using eight radiocarbon ages on aquatic moss macrofossils, which are reliable in this region for radiocarbon dating (52). Macrofossils were sonicated in deionized water and freeze dried prior to preparation (acid–base–acid pretreatment and graphitization) in the Institute of Arctic and Alpine Research (INSTAAR) Laboratory for Accelerated Mass Spectrometry (AMS) Radiocarbon Preparation and Research. Radiocarbon measurements were made at the University of California Irvine AMS facility. The ages were used to create a Bayesian age–depth model in Bacon version 2.3.9.1 for R (53) (mem.strength: 4; mem.mean: 0.9; 116 1-cm sections; *SI Appendix*, Fig. S4), which relies on the IntCal20 calibration curve (54). Interpolated ages were then used to align Holocene DNA samples with pollen samples from a previously published age model (55).

Because internal age control was not possible for the pre-Holocene sediment, we aligned LIG units from core 19CF8-07 with previously published CF8 cores using bulk geochemistry (%C, C:N, and $\delta^{13}C$; see *SI Appendix*). Sediment subsamples were freeze dried, homogenized, and weighed into tin capsules for element analysis. Samples were run on a Flash 2000 Organic Elemental Analyzer interfaced with a Delta V Plus isotope ratio mass spectrometer via a Conflo IV in the University of Colorado Boulder Earth Systems Stable Isotope Lab following standard protocols.

DNA Metabarcoding. Sediment sampling and DNA extractions were completed in an ultra-clean facility dedicated to ancient DNA work at the TrEnD Lab following established ancient DNA protocols for personal protective equipment and tool cleaning. Preparation for PCR was completed in a separate dedicated clean laboratory, and post-PCR work took place in a different building. Pristine sediment samples were taken from the center of the core (by scraping away uppermost sediment and avoiding core tube surfaces). A total of 2 500-mg aliquots were processed from each homogenized sediment subsample.

DNA digestion and extraction were completed following procedures described in Crump et al. (2019). Briefly, each aliquot was treated with 1 mL digest buffer following Grealy et al. (56), vortexed, and incubated in a hybridization oven at 55 °C with rotation for 24 h. An extraction control containing only digest buffer was prepared for each batch of 9 to 11 samples (*SI Appendix*, Table S4). Digests were concentrated to a volume of ∼50 μl using Vivaspin 500 centrifugal concentrators (Sigma Aldrich) and added to 1,300 μl of binding buffer following Dabney et al. (57). Samples were vortexed and then purified using a MinElute PCR Purification Kit (QIAGEN), eluted in a volume of 50 μl and stored at −20 °C.

An initial round of qPCR (StepOnePlus, Applied Biosystems) using full concentration, 1/10, and 1/100 dilution samples targeting the p6 loop of trnL–gh enabled assessment of suitable DNA templates and potential PCR inhibition in all samples. Based on preliminary qPCR results, optimal dilutions (typically 1/10 or 1/100 due to PCR inhibition) were then PCR amplified with unique (never previously used) multiplex identifiers (MID tags) for each metabarcoding assay via single-step amplification. Two PCR replicates were processed for each Holocene extract, and four PCR replicates were processed for LIG and PIG extracts to account for additional DNA degradation in older sediments. Two to four no-template controls and one to two positive controls were processed with each PCR plate. PCR reactions were as described in Crump et al. (2019), using 96-well plates and conditions set for 95 °C for 5 min, followed by 45 cycles of 95 °C for 30 s, 72 °C for 45 s, and 10 min at 72 °C.

The resulting amplicons were combined into "minipools" based on qPCR amplification curves and quantified via QIAxcel fragment analysis (QIAGEN), blended equimolarly into a sequencing library, purified with a QIAquick PCR Purification Kit (QIAGEN), and eluted in a volume of 32 μl. Illumina sequencing adapters were ligated onto the sequencing

libraries using one of two PCR-free ligation methods: the Holocene library was end repaired, A tailed, and ligated using a method described in refs. 32 and 58, with the library purified between each step using a QIAquick PCR Purification Kit (QIAGEN) and eluted in a final volume of 30 μl; LIG libraries were ligated using the NxSeq AmpFREE Low DNA Library Kit (Lucigen) following manufacturer's instructions, with an initial library concentration target of 500 ng and the final library purified using a QIAquick PCR Purification Kit (QIAGEN) and eluted in a volume of 60 μl.

Ligated libraries were size selected using a Pippin Prep (Sage Science) for 150 to 500 bp fragments, then cleaned via QIAquick PCR Purification Kit (QIAGEN). Libraries were quantified via Qubit Fluorometric Quantitation (ThermoFisher Scientific) and QIAxcel fragment analyzer (QIAGEN) to determine ligation efficiency. Dilutions of each library were denatured into single-stranded products and then prepared and loaded on an Illumina MiSeq Reagent Nano Kit version 2 (300 cycles) following manufacturer instruction.

Paired-end sequence data were demultiplexed using the insect package in R (59). Primers, adapters, and tags were then trimmed (exact matches only) and sequences shorter than 30 bp removed using cutadapt version 2.4 (60). Single-end sequences were first processed with OBITools (61): demultiplexed and primers/tags identified and removed (*ngsfilter*), filtered for length (minimum 30 bp; *obigrep*), and split into individual sample files (*obisplit*). All sequences were then dereplicated, denoised, merged (paired end only), and filtered for chimeras using the DADA2 pipeline (62). The resulting amplicon sequence variants were compared against both the National Center for Biotechnology Information (NCBI) GenBank database (63) and a curated Arctic–Boreal–Bryophyte database (64–66) using the BLASTn algorithm (67). Taxonomic assignments were made using a custom LCA algorithm in Python (68), requiring 100% of query coverage and 96% identity match with reference sequences.

Taxonomic assignments were further filtered for presumed contaminants/misassignments based on taxa present in the online version of the Flora of the Canadian Arctic Archipelago (36). Samples (with PCR replicates merged) were only retained if they passed the following final filtering criteria: 1) at least 1,000 reads assigned to ecologically plausible ("local") taxa; 2) more local than contaminant sequences. We completed this filtering process with both the GenBank and curated Arctic–Boreal–Bryophyte database results and discarded a sample if it failed to pass the filter in either case. A minimum read cutoff of 10 reads was used for taxonomic observations, except in cases where a taxon was identified in >10 reads for any of the 12 negative controls, in which case we increased the read cutoff to 100 reads (Salicaceae, *Empetrum*, and *O. Digyna*) to account for low-level cross contamination (*SI Appendix*, Tables S3 and S4). Results derived from the Arctic–Boreal–Bryophyte database comparison were used for subsequent analyses.

We note that the LIG metabarcoding dataset includes two independent batches of sediment samples (overlapping depths from two halves of the same core), which we combined for main figures and interpretation; see *SI Appendix*, text and Fig. S14.

Shotgun Sequencing and Analysis. Five extracts from select intervals of the CF8 core, along with a single library negative control, were prepared into shotgun libraries using a one-reaction, single-stranded library preparation developed to target degraded DNA (69). After adapter ligation, each library was purified using MinElute columns (Qiagen). A qPCR was carried out to determine the number cycles prior to amplifying with Illumina-compatible indices. Each library was subsequently amplified 11 to 18 cycles using 50 μL of Amplitaq 360 Gold Master Mix (ThermoFisher Scientific), 48 μL of DNA input, and 1 μL of 100-μM custom PCR primers containing custom 7-bp barcodes for downstream demultiplexing. Amplified PCR products were then purified using Sera-mag Speed Beads (GE Healthcare Sciences) with a 0.05% Tween concentration and eluted in 24 μL EBT buffer. Fragment size of each purified library was determined using a Fragment Analyzer (Agilent Technologies). Lastly, libraries were sequenced to 300 cycles using an Illumina NextSEq 500 instrument at UC, Santa Cruz Paleogenomics Lab.

Raw sequencing reads were trimmed and merged using SeqPrep (https://github.com/jstjohn/SeqPrep) and subsequently complexity filtered using PrinSEq (70). All complexity filtered reads were aligned to the NCBI full-nucleotide database using the BlastN command line tool and thereafter viewed with MEGAN (MEtaGenome ANalyzer) version 6 (71). Reads were then aligned to several species with readily available complete reference genomes on NCBI using Burrows-Wheeler Aligner (72), allowing each aligned read a minimum mapping quality score of 30. Nucleotide misincorporation plots were generated using MapDamage (73) with reads aligning to *S. brachista*. We note that we used the *S. brachista* genome because it was the highest quality, most complete *Salix* genome available and is genetically similar enough to the *Salix* species native to Arctic Canada to effectively identify *Salix* sequences in our samples. Complete aligned read-length plots accompanied with statistical analysis were generated with R (version 3.6).

Pollen Analysis and July Air Temperature Reconstruction. Standard pollen preparation technique, including dispersion with KOH, digestion with HF and HCl, and acetolysis (74), were applied to 2.0 cm^3 samples of fresh (wet) sediment. Pollen concentrations were determined by spiking with 3 *Lycopodium* spore tablets that contain 18,583 spores each (75). The basic sum used for relative frequency calculations included all spermatophyta taxa. The pollen sum averaged 450 grains in Holocene samples and 550 grains in LIG samples (*SI Appendix*, Table S5). Pollen concentrations were converted from volumetric (grains/cm^3) to concentration by mass (grains/g sediment) using dry bulk density to account for differential compaction between the Holocene and LIG.

July air temperature reconstruction was performed using the modern analog technique (MAT). The reconstruction was made on the basis of a modern database including 828 pollen assemblages from lakes of the Boreal, Subarctic, and Arctic biomes of North America (north of 50°N) and Greenland, and corresponding temperature measurements (76, 77). The temperature data used are from the Climate Research Unit, University of East Anglia gridded climatology based on 1961 to 1990 meteorological averages (78). Pollen data include the 39 most common vascular taxa (18 woody plants and 21 herbs). For MAT, similarity between fossil and modern pollen assemblages is based on the squared chord distance (SCD) (79). In the present study, the adopted SCD threshold below which a modern sample is accepted as an analog is 0.26. To improve the statistical reliability, the July air temperature estimates were based on a set of five closest modern analogs. July air temperature reconstruction was performed with the "bioindic" package (ftp://ftp.cerege.fr/R/Package_bioindic) in R. The accuracy (RMSE) of the reconstruction is estimated to ±1.4 °C (r = 0.92). More details on the MAT approach used are given by ref. 77.

Data Analysis. The Holocene and LIG units were subdivided into biostratigraphic units using constrained hierarchical clustering, computed via *chclust* (coniss method) in the R package Rioja (35). Holocene samples were analyzed using relative abundance of reads assigned to taxa, while LIG samples were analyzed with presence-absence data only; because LIG samples are highly degraded and yielded fewer taxa on average (~2.8 versus 5.7 taxa in the Holocene), the relative abundance of reads is less meaningful and more reasonable results were obtained with presence-absence information only. The number of biostratigraphic units was determined by comparing the dispersion (as within-group sum of squares) between a broken stick model and hierarchical cluster grouping. The crossover point of the two models indicates the number of statistically significant groups based on hierarchical clustering—three groups for both interglacials (*SI Appendix*, Fig. S12) (34). To assess changes in vegetation at the community scale, we conducted nonmetric multidimensional scaling (NMDS) ordination analysis (80) on presence–absence metabarcoding data for the Holocene and LIG combined. NMDS was computed using the R package vegan (81) (*metaMDS*) using a Bray-Curtis dissimilarity matrix, yielding a minimum stress of 0.15.

Data Availability. Sequencing data have been deposited in the Dryad Digital Repository (https://doi.org/10.5061/dryad.pk0p2ngmq) (82) and pollen data have been deposited in the Neotoma Paleocology Database (https://data.neotomadb.org/48940) (83).

ACKNOWLEDGMENTS. We gratefully acknowledge the Qikiqtaani Inuit and government of Nunavut for access to their land (Nunavut Research Institute Permits #0102217R-M and #0203819R-M). We thank CH2MHill Polar Services, Polar Continental Shelf Program, Joshua Akavak, Lasalie Joanasie, Zach Montes, and Devon Gorbey for field support and Mahsa Mousavi Mousaviderazmahalleh and Katrina West for bioinformatics expertise. We thank the INSTAAR Laboratory for AMS Radiocarbon Preparation and Analysis for sample preparation and insights. This research was funded by the US NSF (Office of Polar Programs Awards #1737712 to G.H.M. and J.S., #1737716 to E.K.T., and #1737750 to M.K.R.; NSF Graduate Research Fellowship Program Award #1144083 to S.E.C.; and NSF Doctoral Dissertation Research Improvement Award #1657743 to G.H.M. and S.E.C.), National Geographic Society, CU Center for the Study of Origins, CU Graduate School, and the Geological Society of America.

1. S. C. Elmendorf *et al*., Plot-scale evidence of tundra vegetation change and links to recent summer warming. *Nat. Clim. Chang.* **2**, 8–12 (2012).
2. I. H. Myers-Smith *et al*., Complexity revealed in the greening of the Arctic. *Nat. Clim. Chang.* **10**, 106–117 (2020).
3. Z. A. Mekonnen, W. J. Riley, R. F. Grant, 21st century tundra shrubification could enhance net carbon uptake of North America Arctic tundra under an RCP8.5 climate trajectory. *Environ. Res. Lett.* **13**, 054029 (2018).
4. R. G. Pearson *et al*., Shifts in Arctic vegetation and associated feedbacks under climate change. *Nat. Clim. Chang.* **3**, 673–677 (2013).
5. M. Forkel *et al*., Enhanced seasonal CO2 exchange caused by amplified plant productivity in northern ecosystems. *Science* **351**, 696–699 (2016).
6. M. Sturm, T. Douglas, C. Racine, G. E. Liston, Changing snow and shrub conditions affect albedo with global implications. *J. Geophys. Res.* **110**, 1–13 (2005).
7. F. S. I. Chapin 3rd *et al*., Role of land-surface changes in arctic summer warming. *Science* **310**, 657–660 (2005).
8. A. L. Swann, I. Y. Fung, S. Levis, G. B. Bonan, S. C. Doney, Changes in Arctic vegetation amplify high-latitude warming through the greenhouse effect. *Proc. Natl. Acad. Sci. U.S.A.* **107**, 1295–1300 (2010).
9. D. M. Lawrence, S. C. Swenson, Permafrost response to increasing Arctic shrub abundance depends on the relative influence of shrubs on local soil cooling versus large-scale climate warming. *Environ. Res. Lett.* **6**, 045504 (2011).
10. M. Sturm *et al*., Snow–Shrub interactions in Arctic Tundra: A hypothesis with climatic implications. *J. Clim.* **14**, 336–344 (2001).
11. I. H. Myers-Smith, D. S. Hik, Shrub canopies influence soil temperatures but not nutrient dynamics: An experimental test of tundra snow-shrub interactions. *Ecol. Evol.* **3**, 3683–3700 (2013).
12. B. L. Otto-Bliesner *et al*., How warm was the last interglacial? New model-data comparisons. *Philos. Trans. A Math. Phys. Eng. Sci.* **371**, 20130097 (2013).
13. Members C-LIP, Last Interglacial Arctic warmth confirms polar amplification of climate change. *Quat. Sci. Rev.* **25**, 1383–1400 (2006).
14. D. Dahl-Jensen *et al*.; NEEM community members, Eemian interglacial reconstructed from a Greenland folded ice core. *Nature* **493**, 489–494 (2013).
15. Y. Axford *et al*., Chironomids record terrestrial temperature changes throughout Arctic interglacials of the past 200,000 yr. *Geol. Soc. Am. Bull.* **123**, 1275–1287 (2011).
16. J. M. McFarlin *et al*., Pronounced summer warming in northwest Greenland during the Holocene and Last Interglacial. *Proc. Natl. Acad. Sci. U.S.A.* **115**, 6537–6362 (2018).
17. B. Fréchette, A. P. Wolfe, G. H. Miller, P. J. H. Richard, A. de Vernal, Vegetation and climate of the last interglacial on Baffin Island, arctic Canada. *Palaeogeogr. Palaeoclimatol. Palaeoecol.* **236**, 91–106 (2006).
18. A. M. Yau, M. L. Bender, A. Robinson, E. J. Brook, Reconstructing the last interglacial at Summit, Greenland: Insights from GISP2. *Proc. Natl. Acad. Sci. U.S.A.* **113**, 9710–9715 (2016).
19. E. Post *et al*., The polar regions in a 2°C warmer world. *Sci. Adv.* **5**, eaaw9883 (2019).
20. J. P. Briner, Y. Axford, S. L. Forman, G. H. Miller, P. Wolfe, Multiple generations of interglacial lake sediment preserved beneath the Laurentide Ice Sheet. *Geology* **35**, 887 (2007).
21. E. J. Steig, A. P. Wolfe, G. H. Miller, Wisconsinan refugia and the glacial history of eastern Baffin Island, Arctic Canada: Coupled evidence from cosmogenic isotopes and lake sediments. *Geology* **26**, 835 (1998).
22. G. H. Miller *et al*., Stratified interglacial lacustrine sediments from Baffin Island, arctic Canada: Chronology and paleoenvironmental implications. *Quat. Sci. Rev.* **18**, 789–810 (1999).
23. C. R. Wilson *et al*., Arctic lake ontogeny across multiple interglaciations. *Quat. Sci. Rev.* **31**, 112–126 (2012).
24. H. H. Birks, The Late-Quaternary history of arctic and alpine plants. *Plant Ecol. Divers.* **1**, 135–146 (2008).
25. B. Niemeyer, L. S. Epp, K. R. Stoof-Leichsenring, L. A. Pestryakova, U. Herzschuh, A comparison of sedimentary DNA and pollen from lake sediments in recording vegetation composition at the Siberian treeline. *Mol. Ecol. Resour.* **17**, e46–e62 (2017).
26. L. Parducci *et al*., Ancient plant DNA in lake sediments. *New Phytol.* **214**, 924–942 (2017).
27. M. W. Kerwin, J. T. Overpeck, R. S. Webb, K. H. Anderson, Pollen-based summer temperature reconstructions for the eastern Canadian boreal forest, subarctic, and Arctic. *Quat. Sci. Rev.* **23**, 1901–1924 (2004).
28. N. Polunin, The real arctic: Suggestions for its delimitation, subdivision and characterization. *J. Ecol.* **39**, 308–315 (1951).
29. D. A. Walker *et al*., The Circumpolar Arctic vegetation map. *J. Veg. Sci.* **16**, 267–282 (2005).
30. A. Berger, M. F. Loutre, Insolation values for the climate of the last 10 million years. *Quat. Sci. Rev.* **10**, 297–317 (1991).
31. P. Taberlet *et al*., Power and limitations of the chloroplast trnL (UAA) intron for plant DNA barcoding. *Nucleic Acids Res.* **35**, e14 (2007).
32. S. E. Crump *et al*., Arctic shrub colonization lagged peak postglacial warmth: Molecular evidence in lake sediment from Arctic Canada. *Glob. Change Biol.* **25**, 4244–4256 (2019).
33. M. W. Pedersen *et al*., Postglacial viability and colonization in North America's ice-free corridor. *Nature* **537**, 45–49 (2016).
34. K. D. Bennett, Determination of the number of zones in a biostratigraphical sequence. *New Phytol.* **132**, 155–170 (1996).
35. S. Juggins, rioja: Analysis of Quaternary Science Data (Version 0.9-21, R package, 2017).
36. S. G. Aiken *et al*., *Flora of the Canadian Arctic Archipelago: Descriptions, Illustrations, Identification, and Information Retrieval* (NRC Research Press, National Research Council of Canada, Ottawa, 2007).
37. P. Sjögren *et al*., Lake sedimentary DNA accurately records 20th Century introductions of exotic conifers in Scotland. *New Phytol.* **213**, 929–941 (2017).
38. J. T. Andrews, W. N. Mode, P. J. Webber, G. H. Miller, J. D. Jacobs, Report on the distribution of dwarf birches and present pollen rain, Baffin Island, N.W.T., Canada. *Arctic* **33**, 50–58 (1980).
39. G. H. Miller, J. T. Andrews, S. K. Short, The last interglacial-glacial cycle, Clyde foreland, Baffin Island, N.W.T.: Stratigraphy, biostratigraphy, and chronology. *Can. J. Earth Sci.* **14**, 2824–2857 (1977).
40. A. de Vernal, C. Hillaire-Marcel, Natural variability of Greenland climate, vegetation, and ice volume during the past million years. *Science* **320**, 1622–1625 (2008).
41. M. Edwards, T. Hamilton, S. Elias, N. Bigelow, A. Krumhardt, Interglacial extension of the boreal forest limit in the Noatak valley, Northwest Alaska: Evidence from an exhumed river-cut bluff and debris apron. *Arct. Antarct. Alp. Res.* **35**, 460–468 (2003).
42. A. V. Lozhkin, P. M. Anderson, The last interglaciation in Northeast Siberia. *Quat. Res.* **43**, 147–158 (1995).
43. H. H. Zimmermann *et al*., The history of tree and shrub taxa on bol'shoy Lyakhovsky Island (new siberian Archipelago) since the last interglacial uncovered by sedimentary ancient DNA and pollen data. *Genes (Basel)* **8**, E273 (2017).
44. V. Masson-Delmotte *et al*., "Information from paleoclimate archives in Climate change 2013: The physical science basis. Contribution of working group I to the fifth assessment report of the Intergovernmental panel on climate change" (Cambridge, UK, and New York, NY, 2013).
45. Q. Z. Yin, A. Berger, Individual contribution of insolation and CO2 to the interglacial climates of the past 800,000 years. *Clim. Dyn.* **38**, 709–724 (2012).
46. C. D. Gallup, H. Cheng, F. W. Taylor, R. L. Edwards, Direct determination of the timing of sea level change during termination II. *Science* **295**, 310–313 (2002).
47. M. Crucifix, M. F. Loutre, Transient simulations over the last interglacial period (126-115 kyr BP): Feedback and forcing analysis. *Clim. Dyn.* **19**, 417–433 (2002).
48. G. Schurgers, A. Winguth, The effect of land surface changes on Eemian climate. *Clim. Dyn.* **29**, 357–373 (2007).
49. E. J. Stone, D. J. Lunt, The role of vegetation feedbacks on Greenland glaciation. *Clim. Dyn.* **40**, 2671–2686 (2013).
50. A. Sommers *et al*., "Retreat of the Greenland ice sheet during the last interglacial" in *American Geophysical Union Fall Meeting* (2019).
51. N. J. Rawlence *et al*., Using palaeoenvironmental DNA to reconstruct past environments: Progress and prospects. *J. Quaternary Sci.* **29**, 610–626 (2014).
52. A. P. Wolfe *et al*., "Geochronology of high latitude lake sediments" in *Long-Term Environmental Changes in Arctic and Antarctic Lakes*, R. Pienitz, M. S. V. Douglas, Eds. (Springer, Smol, JP, 2004), pp. 19–52.
53. M. Blaauw, J. A. Christen, Flexible paleoclimate age-depth models using an autoregressive gamma process. *Bayesian Anal.* **6**, 457–474 (2011).
54. P. J. Reimer *et al*., The IntCal20 northern hemisphere radiocarbon age calibration curve (0-55 cal kBP). *Radiocarbon* **62**, 725–757 (2020).
55. Y. Axford, J. P. Briner, G. H. Miller, D. R. Francis, Paleoecological evidence for abrupt cold reversals during peak Holocene warmth on Baffin Island, Arctic Canada. *Quat. Res.* **71**, 142–149 (2009).
56. A. C. Grealy *et al*., A critical evaluation of how ancient DNA bulk bone metabarcoding complements traditional morphological analysis of fossil assemblages. *Quat. Sci. Rev.* **128**, 37–47 (2015).
57. J. Dabney *et al*., Complete mitochondrial genome sequence of a Middle Pleistocene cave bear reconstructed from ultrashort DNA fragments. *Proc. Natl. Acad. Sci. U.S.A.* **110**, 15758–15763 (2013).
58. I. Kozarewa, D. J. Turner, "Amplification-free library preparation for paired-end Illumina sequencing" in *High-Throughput Next Generation Sequencing: Methods and Applications*, Y. M. Kwon, S. C. Ricke, Eds. (Springer Science+Business Media, 2011), 733, pp. 257–266.
59. S. P. Wilkinson, S. K. Davy, M. Bunce, M. Stat, Taxonomic identification of environmental DNA with informatic sequence classification trees. Peer J *Preprints* [Preprint] (2018). 10.7287/peerj.preprints.26812v1. Accessed 31 July 2020.
60. M. Martin, Cutadapt removes adapter sequences from high-throughput sequencing reads. *EMBnet. J.* **17**, 10–12 (2011).
61. F. Boyer *et al*., obitools: A unix-inspired software package for DNA metabarcoding. *Mol. Ecol. Resour.* **16**, 176–182 (2016).
62. B. J. Callahan *et al*., DADA2: High-resolution sample inference from Illumina amplicon data. *Nat. Methods* **13**, 581–583 (2016).
63. D. A. Benson *et al*., GenBank. *Nucleic Acids Res.* **28**, 15–18 (2000).
64. J. H. Sønstebø *et al*., Using next-generation sequencing for molecular reconstruction of past Arctic vegetation and climate. *Mol. Ecol. Resour.* **10**, 1009–1018 (2010).
65. E. Willerslev *et al*., Fifty thousand years of Arctic vegetation and megafaunal diet. *Nature* **506**, 47–51 (2014).
66. E. M. Soininen *et al*., Highly overlapping winter diet in two sympatric lemming species revealed by DNA metabarcoding. *PLoS One* **10**, e0115335 (2015).
67. S. F. Altschul, W. Gish, W. Miller, E. W. Myers, D. J. Lipman, Basic local alignment search tool. *J. Mol. Biol.* **215**, 403–410 (1990).
68. M. Mousavi-Derazmahalleh *et al*., eDNAFlow, an automated, reproducible and scalable workflow for analysis of environmental DNA (eDNA) sequences exploiting Nextflow and Singularity. *Mol. Ecol. Resour.* 10.1111/1755-0998.13356 (2021).
69. C. J. Troll *et al*., A ligation-based single-stranded library preparation method to analyze cell-free DNA and synthetic oligos. *BMC Genomics* **20**, 1023 (2019).
70. R. Schmieder, R. Edwards, Quality control and preprocessing of metagenomic datasets. *Bioinformatics* **27**, 863–864 (2011).
71. D. H. Huson *et al*., MEGAN community edition–Interactive exploration and analysis of large-scale microbiome sequencing data. *PLoS Comput. Biol.* **12**, e1004957 (2016).
72. H. Li, R. Durbin, Fast and accurate short read alignment with Burrows-Wheeler transform. *Bioinformatics* **25**, 1754–1760 (2009).

73. H. Jónsson, A. Ginolhac, M. Schubert, P. L. F. Johnson, L. Orlando, mapDamage2.0: Fast approximate Bayesian estimates of ancient DNA damage parameters. *Bioinformatics* **29**, 1682–1684 (2013).
74. K. Faegri, J. Iversen, *Textbook of Pollen Analysis* (Blackwell Scientific Publications, Oxford, ed. 3, 1975).
75. W. S. Benninghoff, Calibration of pollen and spore density in sediments by addition of exotic pollen in known quantities. *Pollen Spores* **4**, 232–233 (1962).
76. J. Whitmore *et al*., Modern pollen data from North America and Greenland for multi-scale paleoenvironmental applications. *Quat. Sci. Rev.* **24**, 1828–1848 (2005).
77. B. Fréchette *et al*., Methodological basis for quantitative reconstruction of air temperature and sunshine from pollen assemblages in Arctic Canada and Greenland. *Quat. Sci. Rev.* **27**, 1197–1216 (2008).
78. M. New, D. Lister, M. Hulme, I. Makin, A high-resolution data set of surface climate over global land areas. *Clim. Res.* **21**, 1–25 (2002).
79. J. T. Overpeck, T. I. Webb, I. C. Prentice, Quantitative interpretation of fossil pollen spectra: Dissimilarity coefficients and the method of modern analogs. *Quat. Res.* **23**, 87–108 (1985).
80. J. B. Kruskal, Nonmetric multidimensional scaling: A numerical method. *Psychometrika* **29**, 115–129 (1964).
81. J. Oksanen *et al*., vegan: Community Ecology Package, R package version 2.5-6. https://cran.r-project.org/web/packages/vegan/index.html (2019).
82. S. E. Crump *et al*., Ancient plant DNA reveals High Arctic greening during the Last Interglacial. *Dryad Digital Repository*. https://doi.org/10.5061/dryad.pk0p2ngmq. Deposited 27 January 2021.
83. B. Fréchette and S. E. Crump, Dataset 48940. Neotoma Paleocology Database. https://data.neotomadb.org/48940. Deposited 11 February 2021.
84. Y. Axford *et al*., Recent changes in a remote Arctic lake are unique within the past 200,000 years. *Proc. Natl. Acad. Sci. U.S.A.* **106**, 18443–18446 (2009).

PNAS
www.pnas.org

Supplementary Information for

Ancient plant DNA reveals High Arctic greening during the Last Interglacial

Sarah E. Crump[1,2]*, Bianca Fréchette[3], Matthew Power[4], Sam Cutler[2], Gregory de Wet[1,5], Martha K. Raynolds[6], Jonathan H. Raberg[1], Jason P. Briner[7], Elizabeth K. Thomas[7], Julio Sepúlveda[1], Beth Shapiro[2,8], Michael Bunce[4,9], Gifford H. Miller[1]

1. Institute of Arctic and Alpine Research and Department of Geological Sciences, University of Colorado Boulder, Boulder, CO, USA
2. Department of Ecology and Evolutionary Biology, University of California Santa Cruz, Santa Cruz, CA, USA
3. Geotop, Université du Québec à Montréal, Montréal, Quebec, Canada
4. Trace and Environmental DNA (TrEnD) Laboratory, School of Molecular and Life Sciences, Curtin University, Bentley, WA, Australia
5. Department of Geosciences, Smith College, Northampton, MA, USA
6. Institute of Arctic Biology, University of Alaska Fairbanks, Fairbanks, AK, USA
7. Department of Geology, University at Buffalo, Buffalo, NY, USA
8. Howard Hughes Medical Institute, University of California Santa Cruz, Santa Cruz, CA, USA
9. New Zealand Environment Protection Authority, Wellington, New Zealand

* Corresponding author is Sarah E. Crump, 4001 Discovery Dr., Boulder, CO 80303; 651-395-1718

Email: sarah.crump@colorado.edu

https://orcid.org/0000-0002-6606-7350

This PDF file includes:

Supplementary text
Figures S1 to S16
Tables S1 to S5
SI References

Supplementary Information Text

Setting

Lake CF8 (70.55818ºN, 68.94968ºW) is a small lake (surface area 0.05 km^2, max depth ~10 m; Fig. S1) situated at 195 m above sea level on the Clyde foreland, a broad coastal lowland of northeastern Baffin Island (Fig. 1). Its small catchment (~0.2 km^2) is typical of a High Arctic tundra (1, 2) or Arctic Bioclimate Subzone C (3). The modern plant community includes rare prostrate dwarf willow (*Salix*) in a predominantly herbaceous tundra vegetation (Fig. S2). The mean annual temperature at nearby Clyde River (18 km to the southeast) is -12.6ºC, with monthly averages ranging from -29.9ºC (February) to +5.0ºC (July) (1981 to 2010 Canadian Climate Normals, Environment Canada: http://climate.weather.gc.ca). Bedrock in the region is composed of Precambrian granite and gneiss.

Core alignment and chronology

Because internal age control was not possible for the pre-Holocene sediment, we aligned LIG units from core 19CF8-07 with previously published CF8 cores using bulk geochemistry (%C, C:N, and δ^{13}C; Fig. S3). Composite depths were adjusted to align a prominent uptick in C:N between 220 and 230 cm composite depth. All three geochemical parameters aligned well for the peak LIG, so the adjusted composite depths were used to compare pollen (analyzed in the same core, 04-CF8-02, as bulk geochemistry measurements were made) with DNA data from 19CF8-07. Adjusted composite depths are used in all figures and tables.

We note that one OSL age reported in Briner et al. (2007) contained a typo indicating a smaller uncertainty than another date from the exact same interval (05-CF8-01 90–95 cm). We have updated that uncertainty from 1 ka to 10 ka in Fig. 2 based on discussion with the original authors.

Shotgun sequencing results

To verify the authenticity of the plant DNA within the LIG unit, we conducted shotgun sequencing on a subset of five samples (see *Methods*). Three of the five extracts (one Holocene and two LIG) yielded sufficiently complex libraries and read coverage (just over two million raw reads each), of which 50-96% of reads passed bioinformatic filtering. We aligned filtered reads to NCBI's complete nucleotide reference database and found that domain-level sample composition was similar among the three samples, averaging 85% Bacteria, 5% Archaea, and 9% Eukaryota (Fig. S15). In the LIG samples, 46% of Eukaryota were assigned to Viridiplantae, whereas only 19% of eukaryotic reads in the Holocene were assigned to Viridiplantae.

Authenticity of sedaDNA

A variety of evidence supports the notion that the DNA analyzed from the CF8 sediment core is endogenous and ancient. We summarize those lines of evidence below:

- The vegetation history based on trnL p6 loop metabarcoding align well with ecological and paleoclimatic predictions. The taxa that are unique to the LIG are more cold-intolerant, while taxa unique to the Holocene are relatively hardy, consistent with generally cooler conditions in the Holocene (Fig. S2). The temporal patterns within each interglacial (Fig. 3) are consistent with summer insolation forcing—peak warmth early and gradual cooling through the middle and late part of the interglacial—with some evidence for vegetation lags.
- The dominant taxa and appearance of *Betula* in the middle LIG unit are consistent with both the CF8 pollen record (Fig. S11) as well as other pollen records from the region (4). The relative scarcity of *Betula* reads in LIG sediment is expected based on its somewhat long trnL p6 loop amplicon length (61 bp) compared to that of other Arctic plants (Fig. S16) and the full distribution of DNA fragment lengths in these samples (Figs. S8–S10), indicating a paucity of suitable templates in this ancient sediment. We note that the somewhat longer overall fragment lengths in Holocene samples (Fig. S10) and the detection of taxa with longer trnL p6 loop amplicon length (e.g., *Eriophorum*, 82 bp) suggest that if *Betula* were present in the Holocene, we would have detected it.

- The primary temporal patterns and dominant plant taxa within the LIG were confirmed by a second round of metabarcoding conducted on independent samples from the archive half of the CF8 core (Fig. S14). For the second round of metabarcoding analyses, the same protocols were followed except that we eliminated freeze-thaw cycles where possible, particularly between subsampling and extraction. By proceeding directly from sampling to digestion and extraction (rather than storing at -20ºC in between), we infer that additional DNA damage was mitigated, increasing the rate of passing our quality filter from 59.1% to 80.6% and increasing the average taxa per sample from 2.1 to 3.2. General corroboration of the key taxa and stratigraphic patterns in our quality-filtered data lends confidence that the primary signal is that of endogenous DNA.
- Extraction controls across all batches from Lake CF8 contain few arctic taxa and at low read numbers (Table S4). By sequencing all extraction controls, we were able to customize our quality filtering (e.g., minimum read cutoffs) to ensure a conservative approach to removing possible contamination. Extraction controls amplified consistently later than sediment samples in PCR, with average cycle threshold (C_T) values >4 units higher than sediment samples, which had an average C_T value of 33.8 ± 2.6 (mean ± 1 SD) across all replicates. This is consistent with sediment samples containing endogenous, amplifiable DNA.
- The decrease in proportion of samples that passed our final quality filter from the Holocene (89%) to the LIG (72%) to the PIG (8%) (Fig. 2), as well as a decrease in taxonomic richness between interglacials (Fig. S5), is consistent with the degradation of endogenous sedimentary DNA rather than modern contamination.
- Shotgun sequencing of two LIG samples and one Holocene sample reveal diagnostic damage patterns consistent with their ancient origin. For reads aligned to a complete *Salix* reference genome, fragment ends featured the expected C to T and G to A transitions that are characteristic of degraded DNA (Figs. S6 and S7). Aligned reads, as well as the total sedimentary DNA pool, were characteristically short (Figs. S8-10).

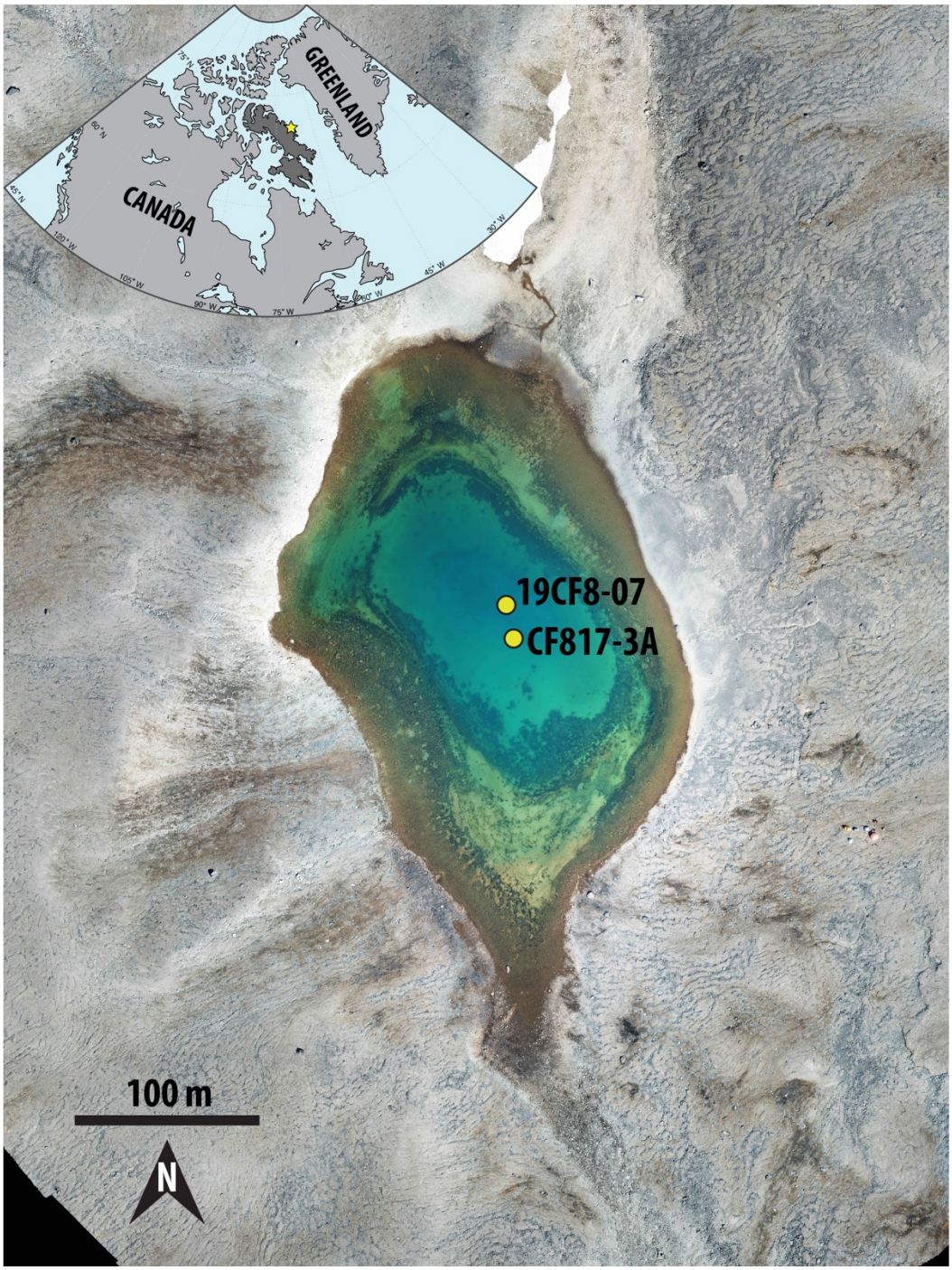

Fig. S1. Drone image of Lake CF8 from August 2019 showing locations of 2017 (Holocene) and 2019 (LIG) sediment cores. Imagery was captured with a DJI Mavic Pro drone (4 cm resolution) and stitched together with Maps Made Easy online software (https://www.mapsmadeeasy.com/).

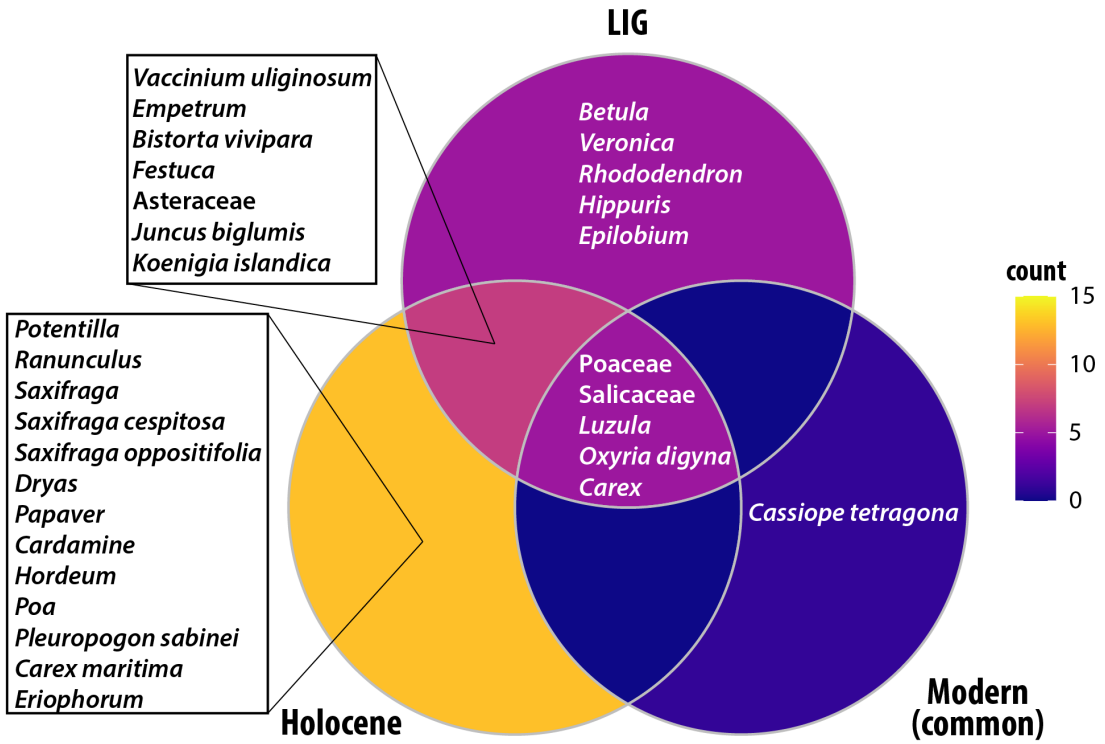

Fig. S2. Venn diagram of taxa present in each interglacial (based on metabarcoding data) as well as the modern catchment. The color of each region of the diagram corresponds to the number of taxa included in that region, using the "count" color scale shown. Common and occasional vascular plant taxa in the modern catchment were included at the taxonomic level that is resolvable with trnL p6 metabarcoding (e.g., *Salix herbaceae* included at family level, Salicaceae).

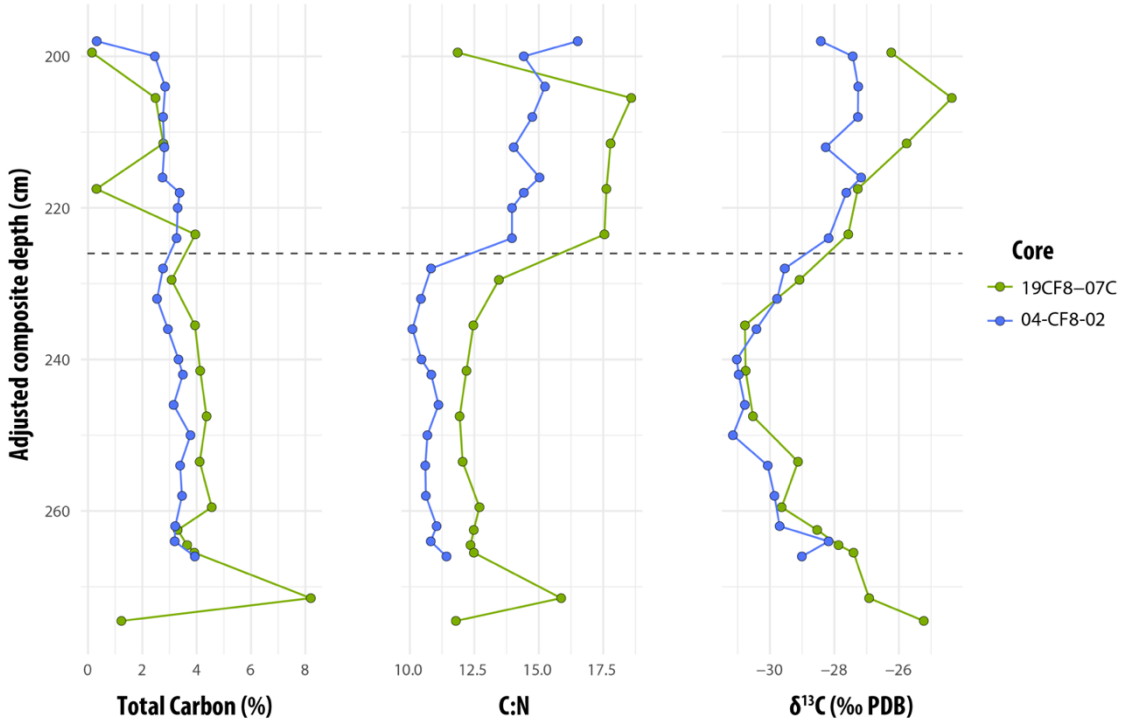

138

139 **Fig. S3.** Alignment of CF8 LIG units from older (04-CF8-02) and newer (19CF8-07C) cores using
140 bulk geochemistry. Dashed line indicates depth of prominent shift in C:N ratio used to align
141 composite depths.
142
143

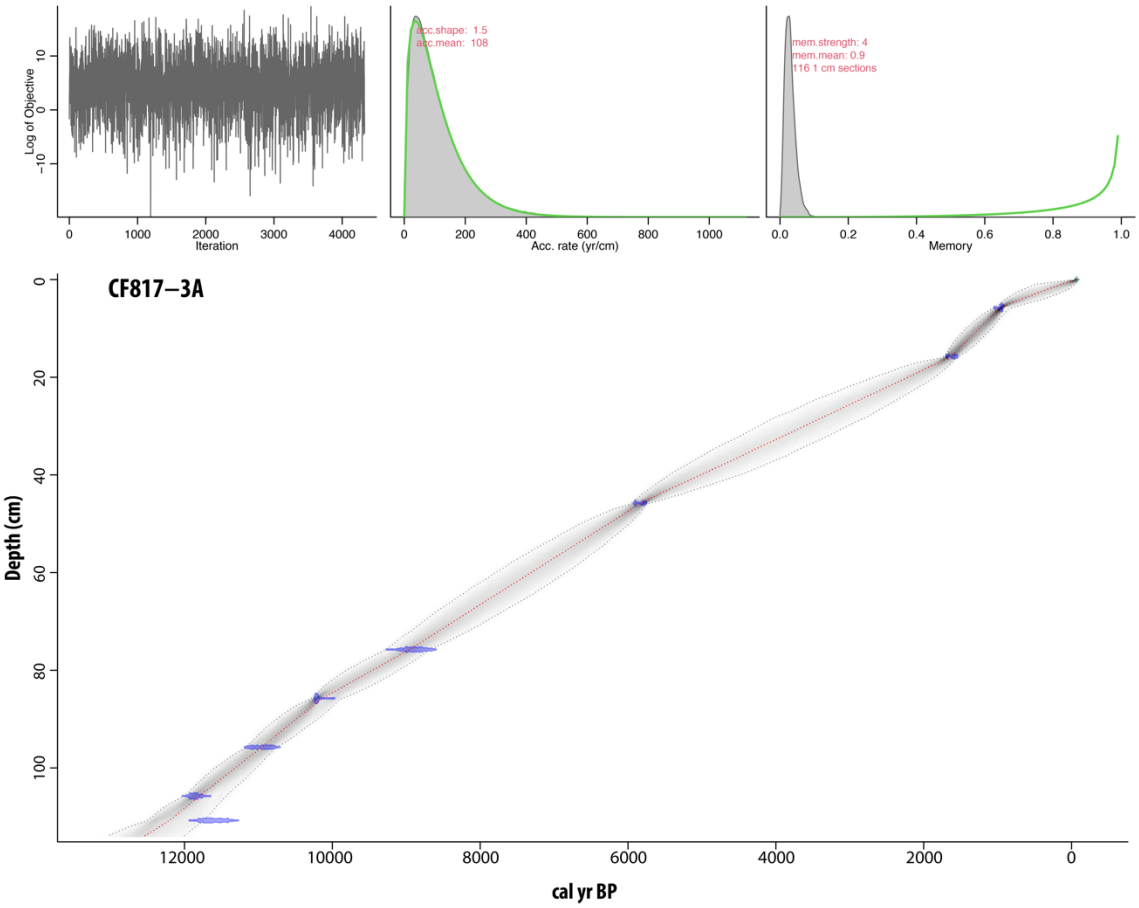

Fig. S4. Holocene age model based on eight radiocarbon dates (blue markers) from macrofossils (Table S2), computed using R package Bacon, version 2.3.9.1 (5). The surface age (green marker) was set as the year of collection (2017 CE or -67 yr BP) because the core included the sediment-water interface.

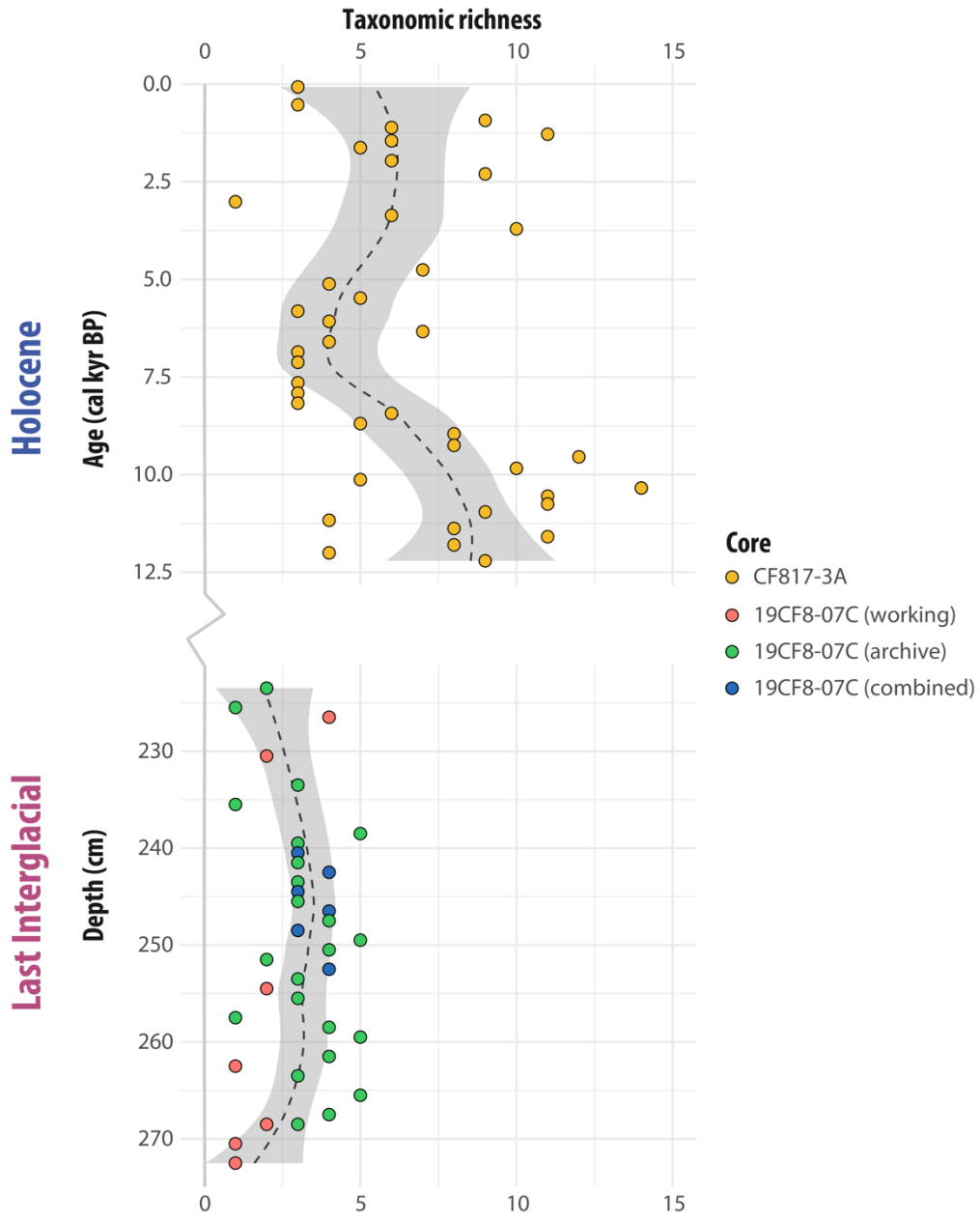

151

152 **Fig. S5.** Taxonomic richness downcore based on trnL p6 loop metabarcoding. Dashed lines are
153 loess smoothing functions (span = 0.8) with 95% confidence interval (gray shading) computed in
154 the R package ggplot2 (6). Taxonomic richness is shown for samples that passed final quality
155 filtering, following all filtering steps. Data from samples taken from the same depth interval in
156 working and archive halves of core 19CF8-07C were combined (blue markers). See *Materials*
157 *and Methods* for more detail.

158

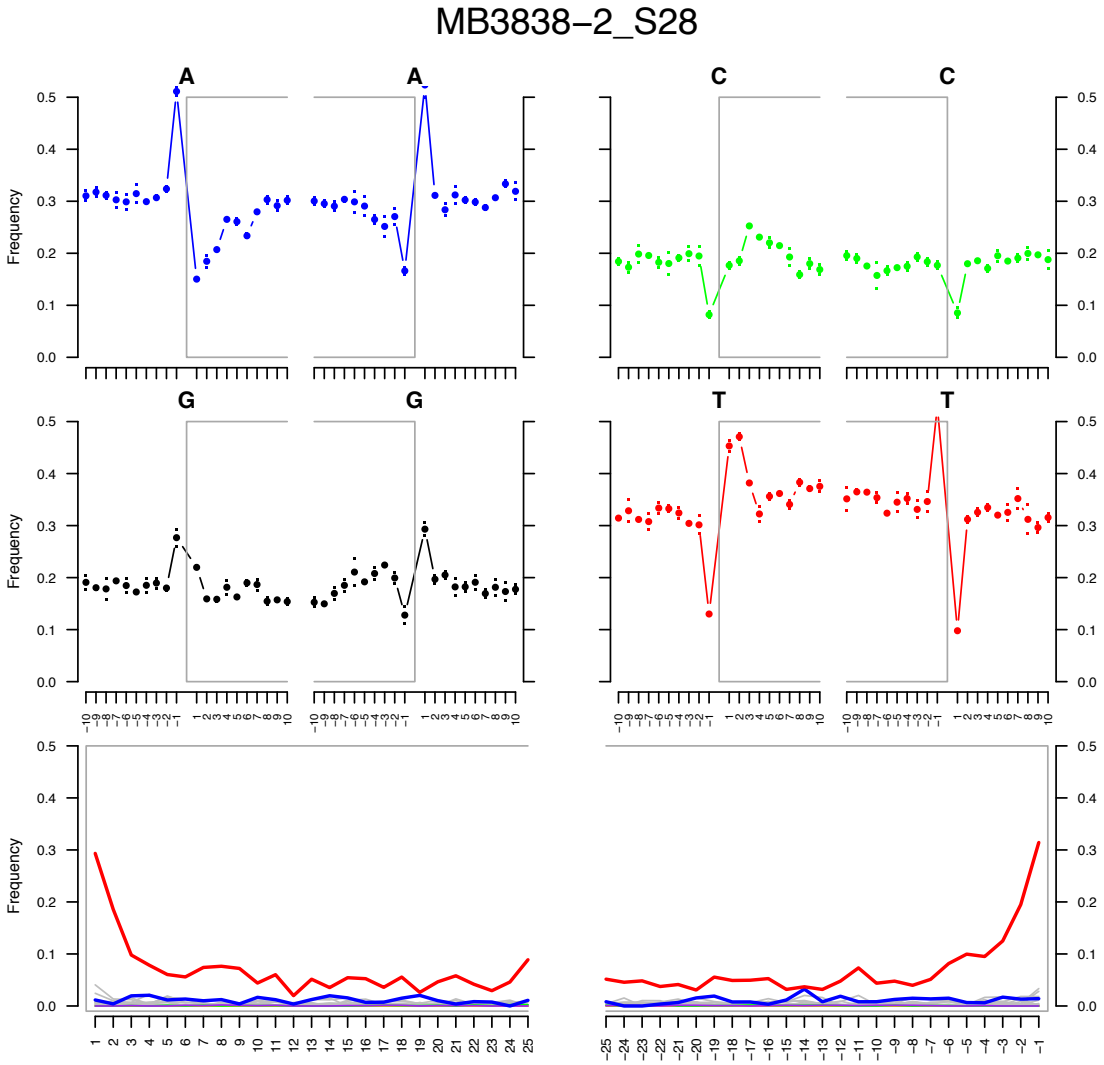

Fig. S6. *MapDamage* nucleotide frequency and misincorporation plots for sample MB 3838 (LIG, depth = 242.5 cm) for reads aligned to the *Salix brachista* genome. Top four panels show base frequency along the read (denoted by gray box) and outside the read. Bottom panel shows specific misincorporations from the 5' (left) and 3' (right) end of reads. Red line shows C to T substitutions, blue line shows G to A substitutions, and grey lines show all other substitutions.

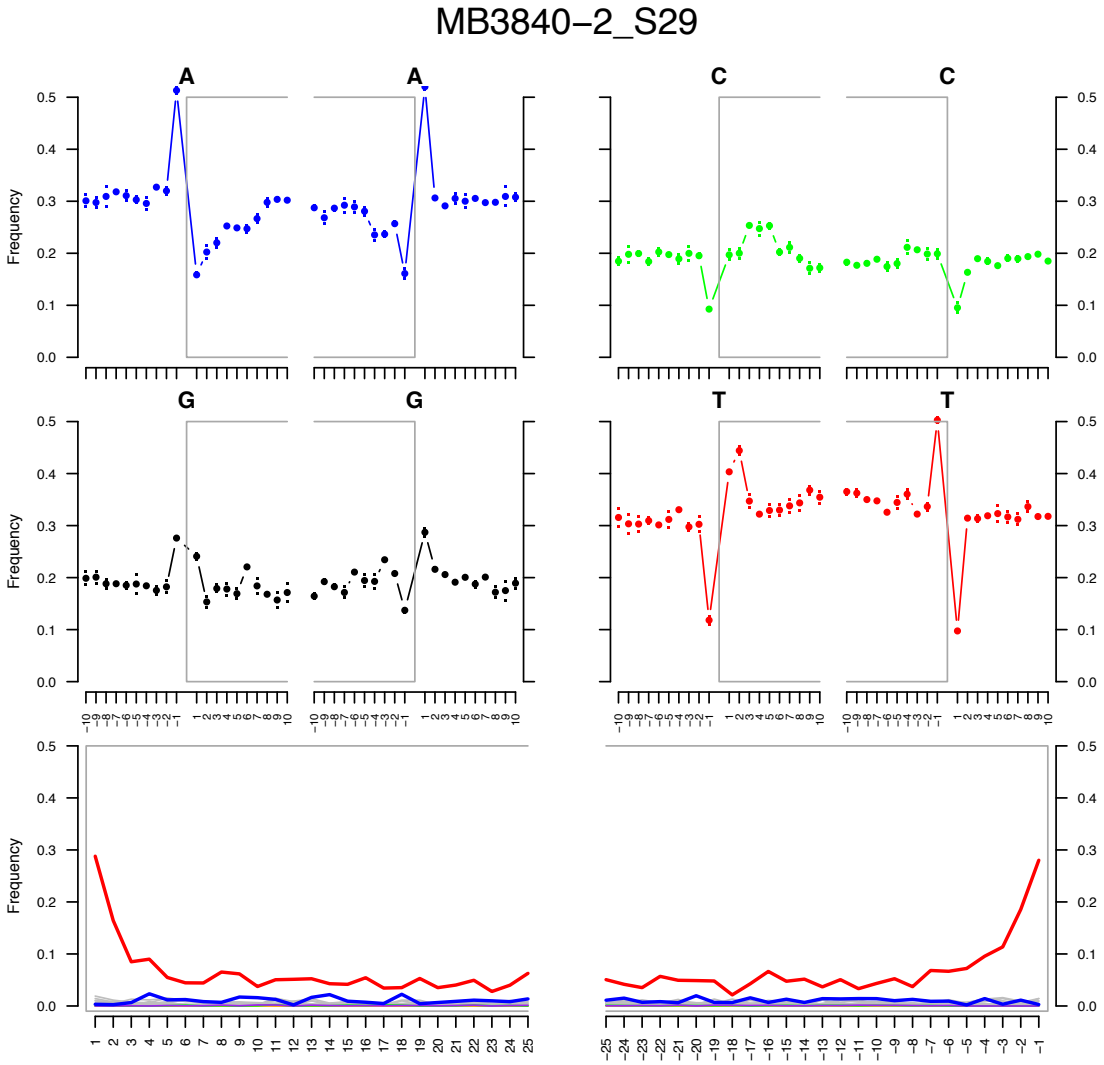

Fig. S7. *MapDamage* nucleotide frequency and misincorporation plots for sample MB 3840 (LIG, depth = 246.5 cm) for reads aligned to the *Salix brachista* genome. Top four panels show base frequency along the read (denoted by gray box) and outside the read. Bottom panel shows specific misincorporations from the 5' (left) and 3' (right) end of reads. Red line shows C to T substitutions, blue line shows G to A substitutions, and grey lines show all other substitutions.

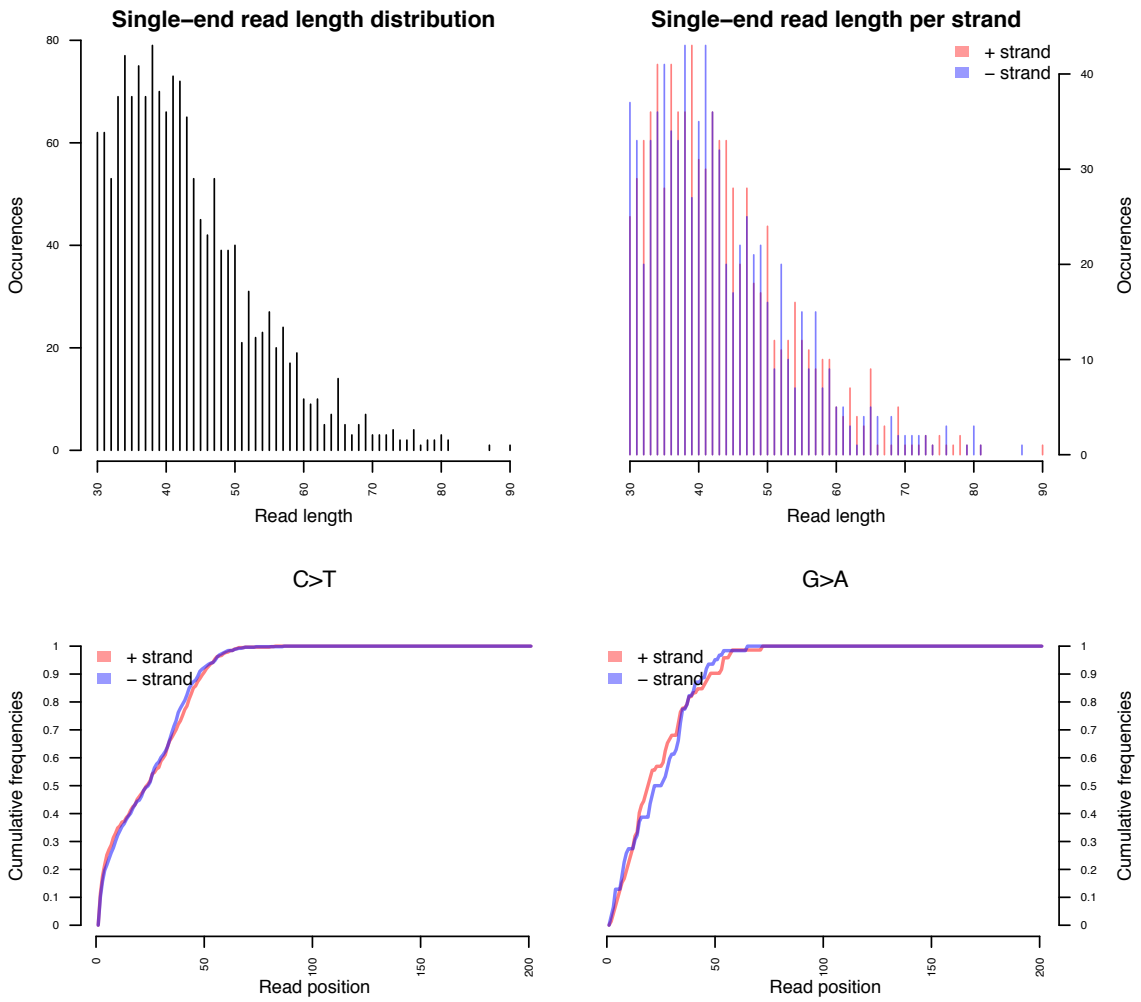

Fig. S8. Fragment length distributions and nucleotide misincorporation patterns from sample MB 3838 (LIG, depth = 242.5 cm) for reads aligned to the *Salix brachista* genome.

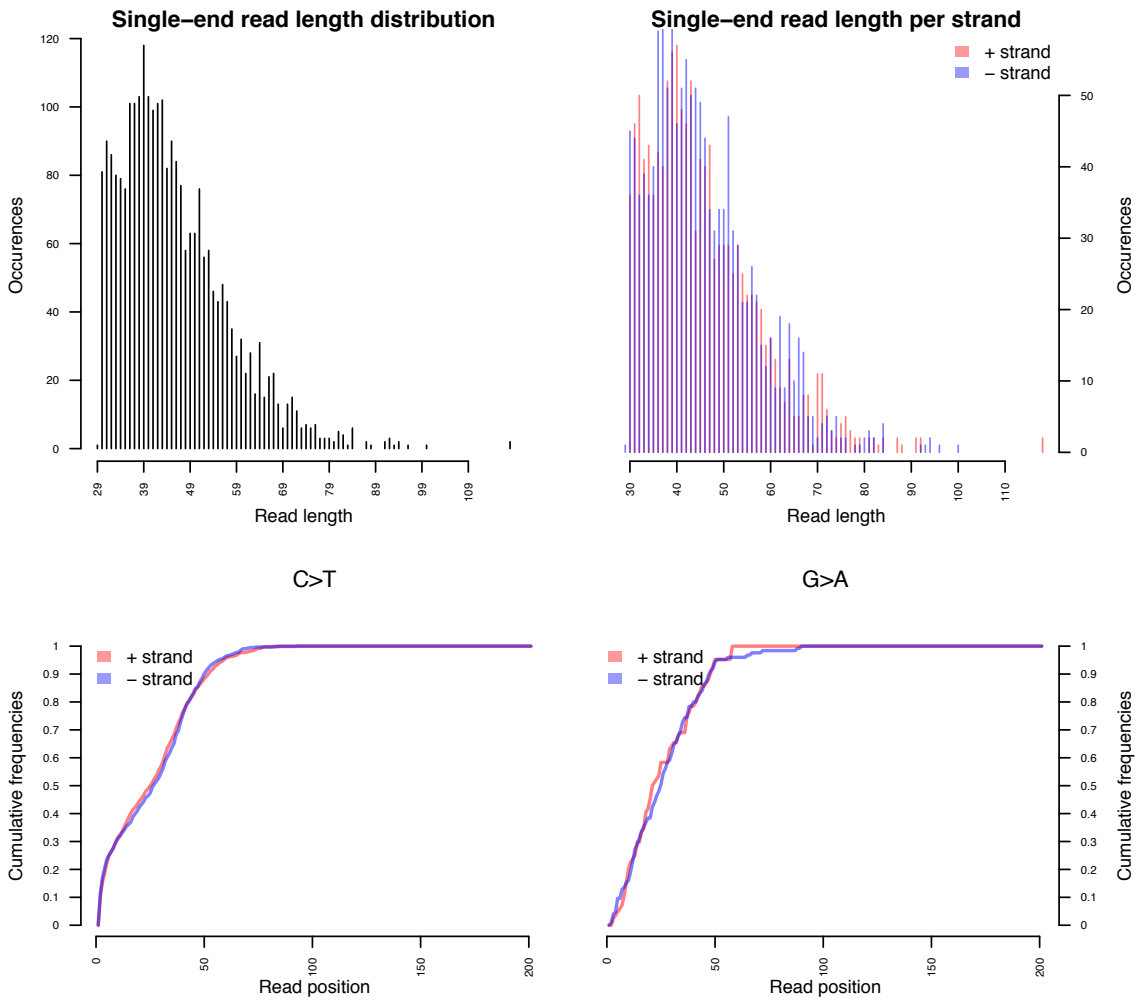

177

178 **Fig. S9.** Fragment length distributions and nucleotide misincorporation patterns from sample MB
179 3840 (LIG, depth = 246.5 cm) for reads aligned to the *Salix brachista* genome.
180

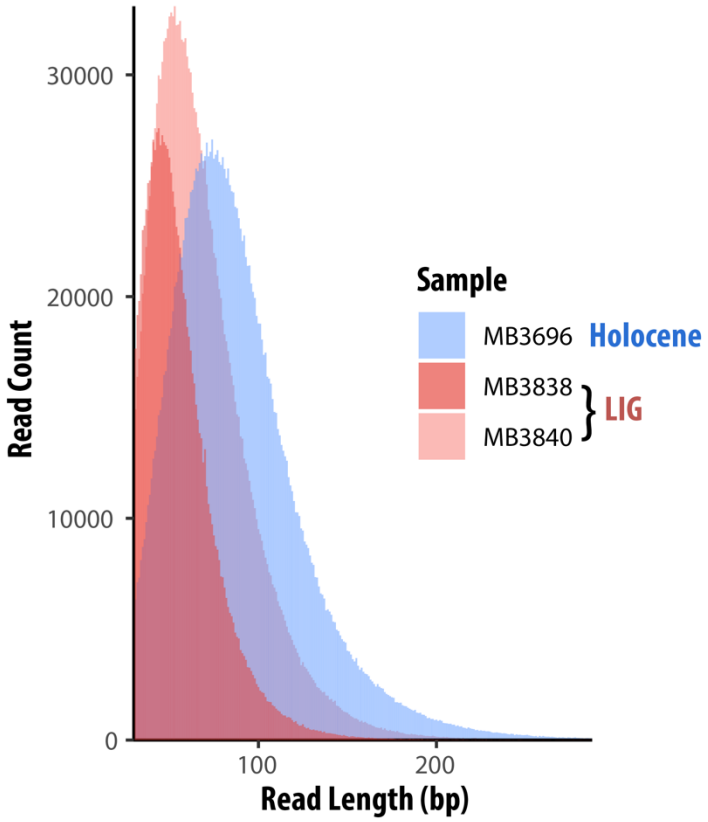

Fig. S10. Fragment length distributions for all reads that passed bioinformatic filtering based on shotgun sequencing. Sample MB 3696 is from the early Holocene (9.5 ka), while samples MB 3838 and 3840 are from the LIG (depths = 242.5 cm and 246.5 cm).

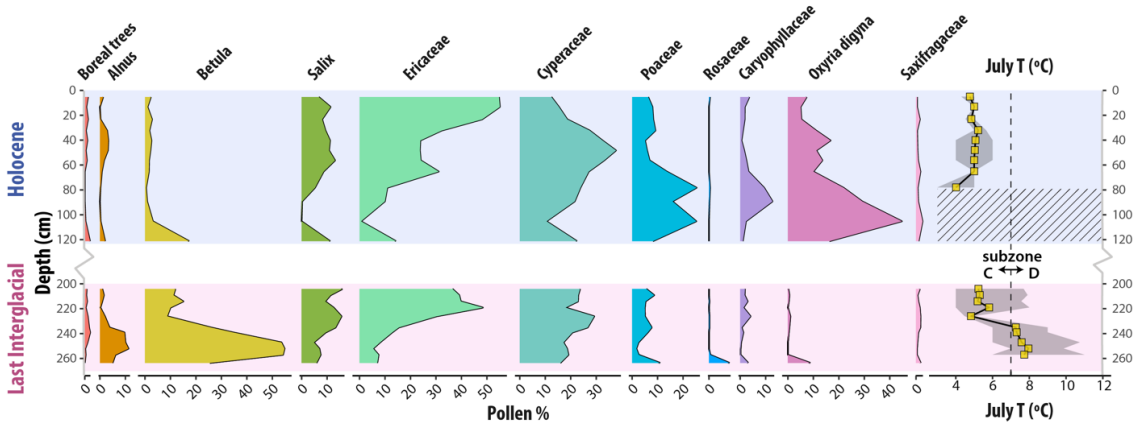

Fig. S11. Lake CF8 summary pollen diagram for the Holocene and LIG. Taxa curves represent relative abundance of pollen grains for each sample. Pollen-inferred July air temperature estimate is based on the modern analogue technique and includes the temperature range (gray band) from the five best modern analogues (see *Materials and Methods*). Dashed line indicates mean July temperature threshold (7ºC) defining the boundary between subzones C and D. Hatched area denotes interval with no adequate modern analogue.

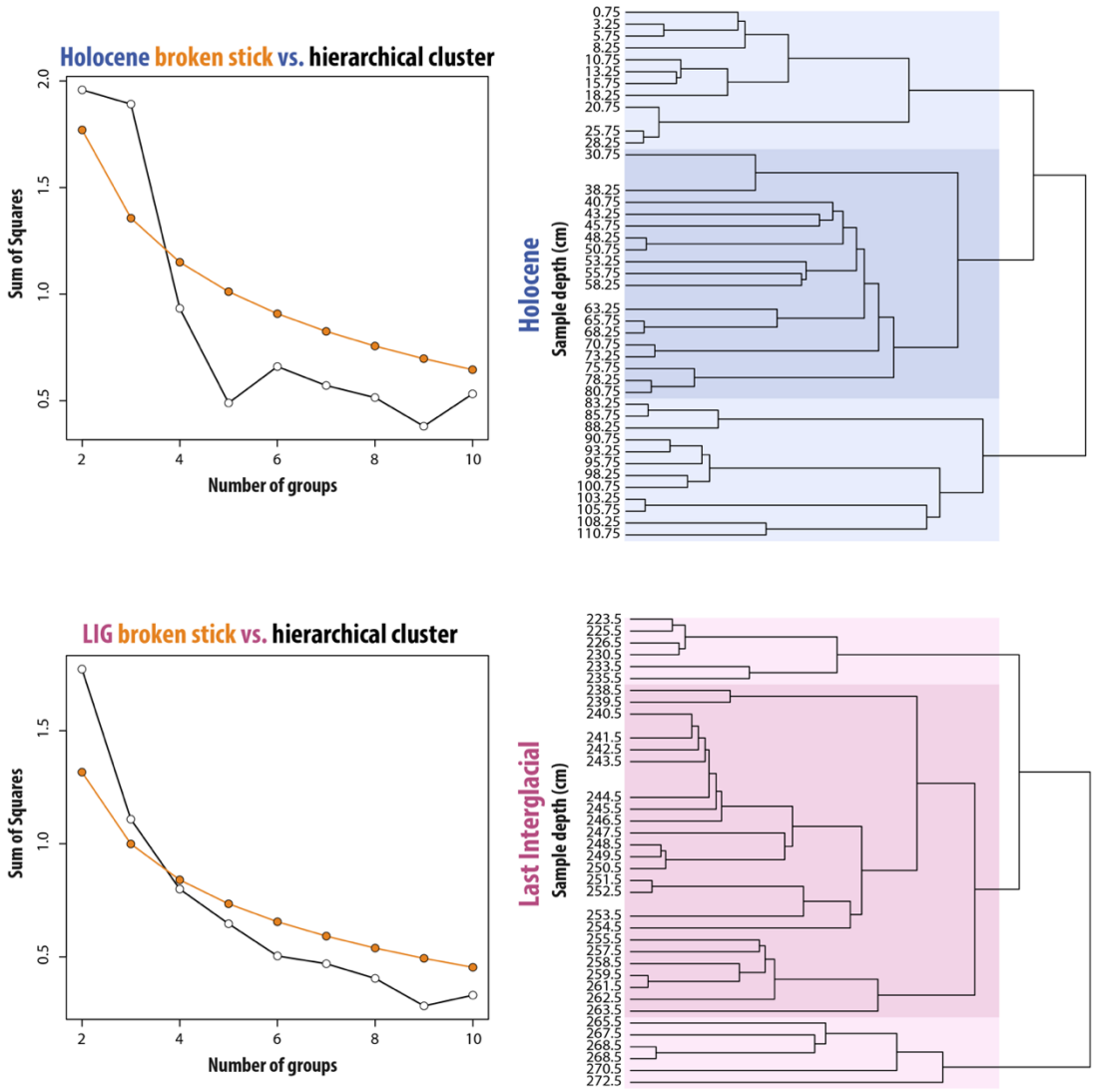

Fig. S12. Constrained hierarchical clustering results for the Holocene (upper; relative abundance of reads assigned to taxa) and LIG (lower; presence-absence of taxa) metabarcoding data. Left panel shows a comparison of dispersion between a broken stick model and hierarchical cluster grouping as within-group sum of squares for a given number of groups. The number of statistically significant groups based on hierarchical clustering is determined by the crossover point of the two curves, which indicate three significant groups for both interglacials. Right panel includes dendrograms from constrained hierarchical clustering based on Bray-Curtis dissimilarity matrices, constrained by sample stratigraphic order. Colored boxes highlight the three significant biostratigraphic units determined by the analysis. All analyses were conducted using the R package rioja (*chclust* function, *coniss* method) (7, 8).

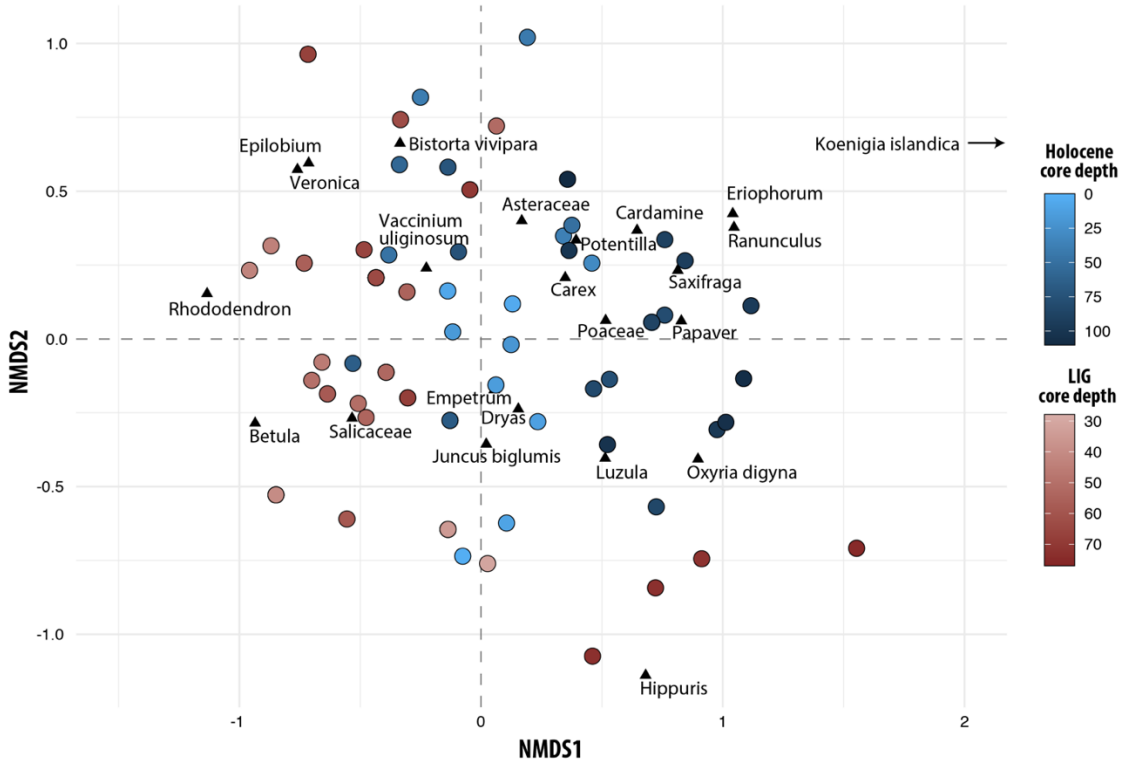

Fig. S13. NMDS biplot of presence-absence metabarcoding data for Holocene (blue) and LIG (red) samples, with color scale indicating depth within sediment core. Taxa loadings are indicated with black triangles. We note that *Koenigia islandica* (and the lowest/oldest LIG sample) plotted off the scale as indicated. Taxa within Poaceae, Saxifraga, and Carex were summed for the analysis. NMDS was computed using the metaMDS function in the R package vegan (9) using a Bray-Curtis dissimilarity matrix, yielding a minimum stress of 0.15. Early samples within each interglacial (darker symbols) generally have a higher score on the first axis (NMDS1) than later samples, indicating coherent temporal patterns across interglacials.

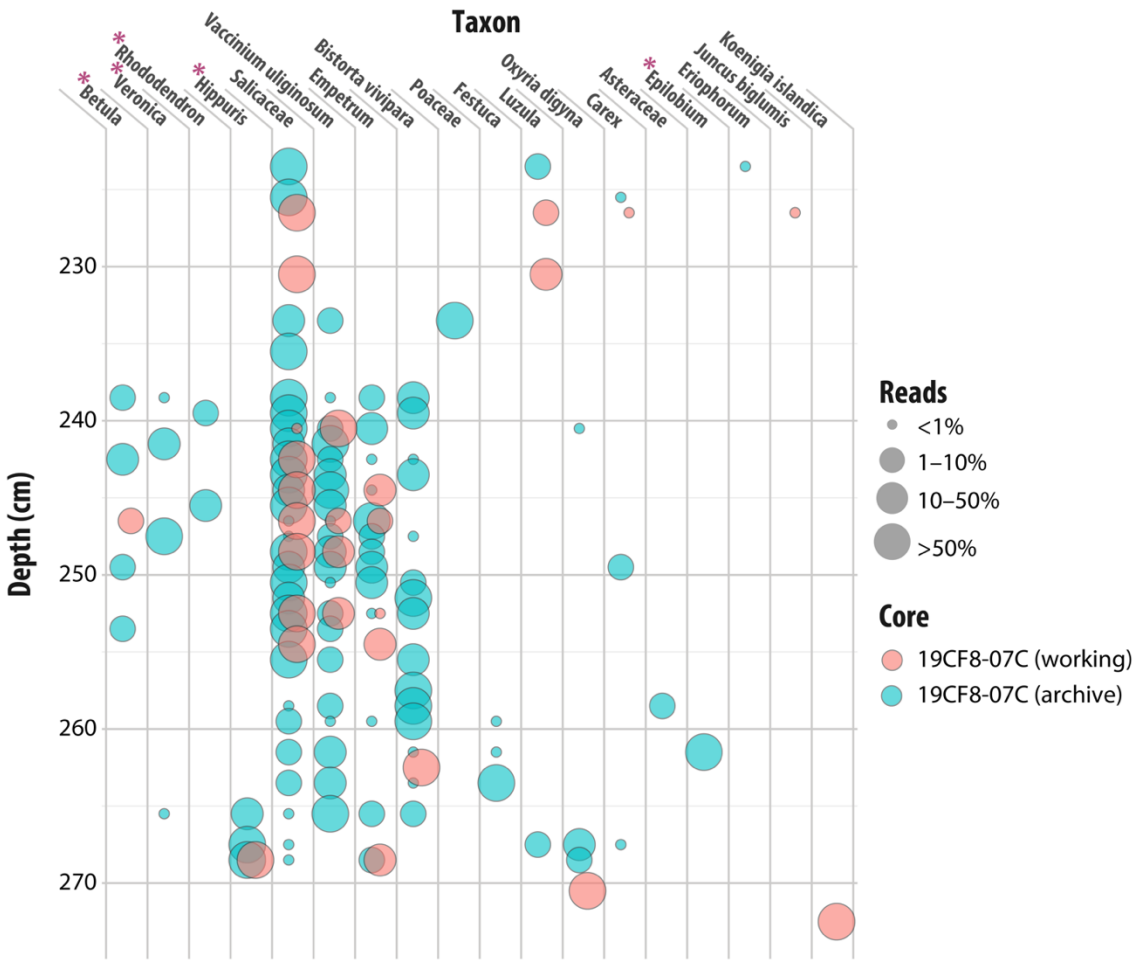

Fig. S14. Comparison of first (pink) and second (blue) rounds of LIG metabarcoding analyses, using independent samples from separate core halves. Symbols have been horizontally offset to aid in visualization. Taxa names with a pink asterisk are those that only occur in the LIG.

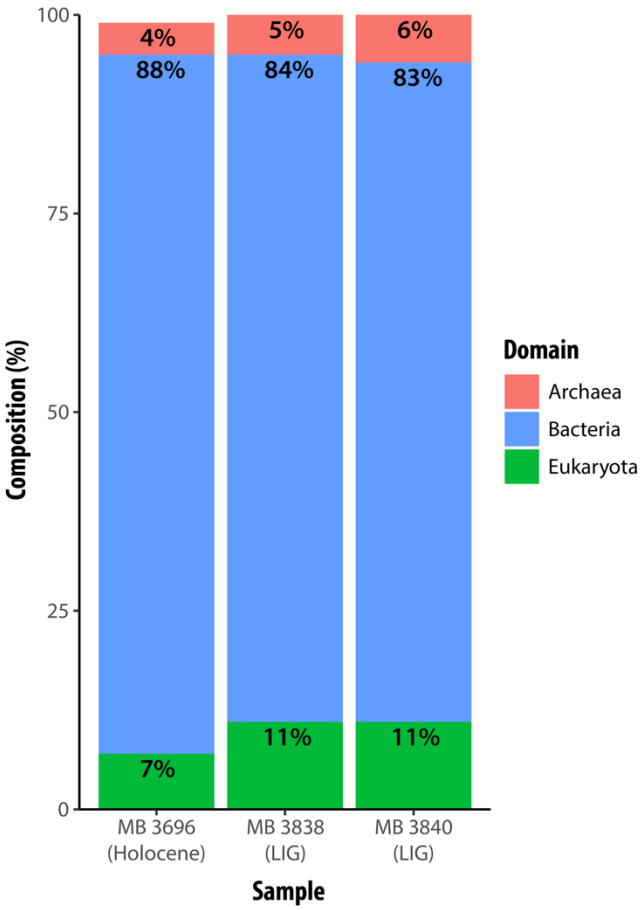

Fig. S15. Domain-level composition of Lake CF8 sediment extracts based on shotgun sequencing. Sample MB 3696 is from the early Holocene (9.5 ka), while samples MB 3838 and 3840 are from the LIG (depths = 242.5 cm and 246.5 cm).

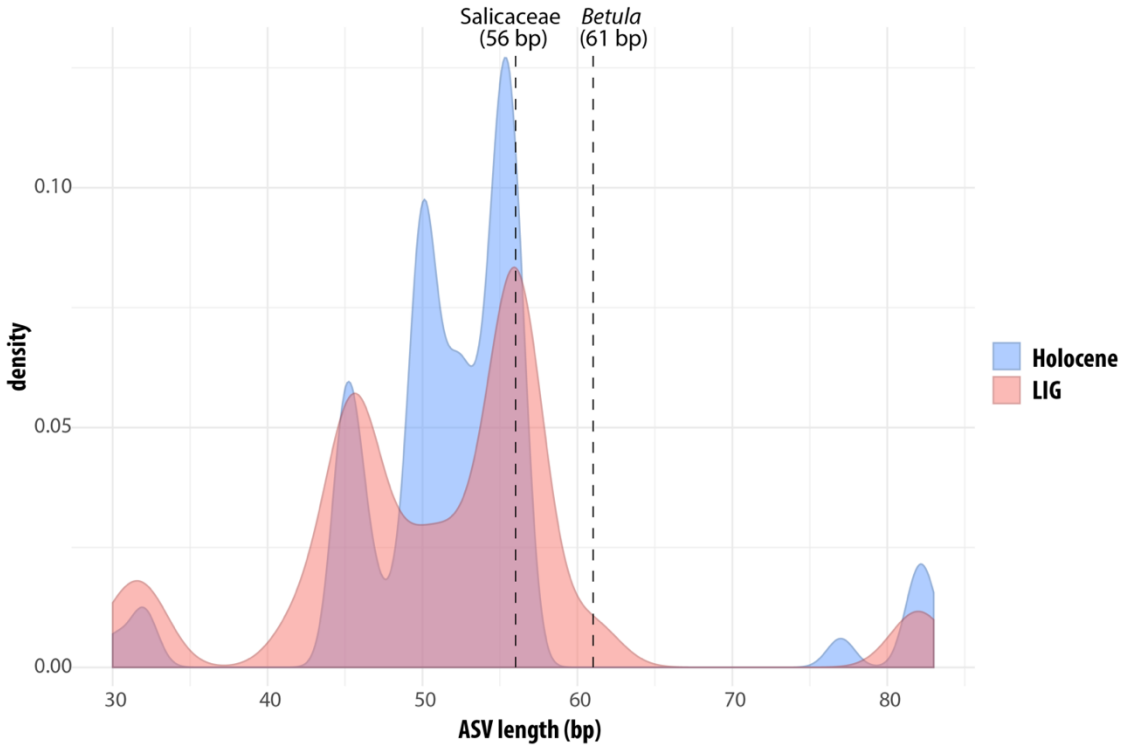

Fig. S16. Distribution of amplicon sequence variant (ASV) lengths for trnL p6 loop metabarcoding across the Holocene and LIG units, shown as kernel density estimates computed in the R package ggplot2 (6). The sequence length for key woody taxa (Salicaceae and *Betula*) are shown as dashed lines. Only ASVs assigned to arctic taxa that passed final quality filtering were included in the analysis. The distributions show that there was no systematic bias in taxa detection in the LIG compared to the Holocene due to a higher level of DNA degradation. Minor differences in these curves results from differences in actual plant occurrence between the interglacials (e.g., *Betula* [61 bp] only in the LIG and *Dryas* [51 bp] in the Holocene).

Table S1. Metadata for Fig. 1 temperature records

Site	Proxy	Baseline (yr CE)	Season	T anomaly (+ ºC)	Reference
Wax Lips Lake (WLL)	Chironomids	1952-2014	July	7 ± 1.7	McFarlin et al. (2018)[10]
NEEM ice core	Air $\delta^{15}N$	Preindustrial	Annual	9 ± 2	Landais et al. (2016)[11]
GISP2 ice core	Ice $\delta^{18}O$	1000-2000	Annual	6 ± 2	Yau et al. (2016)[12]
NGRIP ice core	Ice $\delta^{18}O$	unspecified	Annual	≥5	NGRIP Members (2004)[13]
Lake CF8 (CF8)	Chironomids	1961-1990	July	4 to 5 ± 2.2	Axford et al. (2011)[14]
Fog Lake (FOG)	Chironomids	1971-2000	July	3 to 4 ± 1.5	Francis et al. (2006)[15]
Fog Lake (FOG)	Pollen	1971-2000	July	4 to 5 ± 1.2	Fréchette et al. (2006)[16]
Brother-of-Fog Lake (BRO)	Chironomids	1971-2000	July	8 to 9 ± 1.5	Francis et al. (2006)[15]
Brother-of-Fog Lake (BRO)	Pollen	1971-2000	July	3 to 4 ± 1.2	Fréchette et al. (2006)[16]
Amorak Lake (AKL)	Pollen	1971-2000	July	4 to 5 ± 1.2	Fréchette et al. (2006) [16]
Robinson Lake (ROB)	Pollen	unspecified	July	5	Miller et al. (1999)[17], CAPE members (2006)[18]
Flitaway/Isortoq Beds (ISO)	Beetles, plants	unspecified	Annual	4 to 5	Morgan et al. (2003)[19], CAPE members (2006)[18]

Table S2. Radiocarbon data for Lake CF8 cores

Lab ID	Core	Unit	Core depth (cm)	Composite depth (cm)	Sample type	Conventional age (14C yr BP)	Uncertainty (14C yrs)	Median calibrated age (cal yr BP)*	–2 sigma (cal yr BP)	+ 2 sigma (cal yr BP)
NSRL-36383	CF817-3A-1B-02	Holocene	5-6.5	5.75	Aquatic macrofossil	1,060	±20	949	925	1,051
NSRL-36384	CF817-3A-1B-02	Holocene	15-16.5	15.75	Aquatic macrofossil	1,715	±25	1,600	1,538	1,697
NSRL-36385	CF817-3A-1B-02	Holocene	45-46.5	45.75	Aquatic macrofossil	5,110	±25	5,811	5,752	5,923
NSRL-36386	CF817-3A-1B-02	Holocene	75-76.5	75.75	Aquatic macrofossil	8,040	±80	8,894	8,605	9,194
NSRL-36387	CF817-3A-1B-02	Holocene	85-86.5	85.75	Aquatic macrofossil	9,035	±40	10,213	9,971	10,250
NSRL-36388	CF817-3A-1B-02	Holocene	95-96.5	95.75	Aquatic macrofossil	9,605	±45	10,941	10,764	11,171
NSRL-36389	CF817-3A-1B-02	Holocene	105-106.5	105.75	Aquatic macrofossil	10,195	±40	11,864	11,653	11,995
NSRL-36390	CF817-3A-1B-02	Holocene	110-111.5	110.75	Aquatic macrofossil	10,080	±60	11,626	11,336	11,874
NSRL-38260	19CF8-07A	Interstadial	52-54	161	Aquatic macrofossil	>46700	n/a	n/a	n/a	n/a
NSRL-38259	19CF8-07C	LIG	77-80	273.5	Aquatic macrofossil	46,100	±2,300	48,927	44,790	n/a

[a]Calibrated using CALIB 8.20[20] with the IntCal20 calibration curve[21]

Table S3. Metabarcoding data (read numbers) for Lake CF8 cores

Core[a]	Composite depth (cm)	Post-filter reads	Pre-filter reads	Betula[b]	Veronica	Rhododendron	Hippuris	Salicaceae	Vaccinium uliginosum	Empetrum	Bistorta vivipara	Poaceae	Festuca	Hordeum	Poa	Pleuropogon sabinei	Luzula	Oxyria digyna	Carex	Carex maritima	Asteraceae	Epilobium	Eriophorum	Juncus biglumis	Koenigia islandica	Potentilla	Ranunculus	Saxifraga	Saxifraga cespitosa	Saxifraga oppositifolia	Dryas	Papaver	Cardamine
CF817-3A	0.75	16376	18159	0	0	0	0	13682	2667	0	27	0	0	0	0	0	0	0	0	0	0	0	0	0	0	0	0	0	0	0	0	0	0
CF817-3A	3.25	7570	7623	0	0	0	0	2615	0	0	0	0	0	0	0	0	4933	0	0	0	0	0	0	0	0	0	0	0	0	0	22	0	0
CF817-3A	5.75	7554	7554	0	0	0	0	1377	1020	0	69	0	0	0	0	0	3458	0	0	0	0	0	0	60	0	0	0	94	0	383	0	0	1022
CF817-3A	8.25	24958	25049	0	0	0	0	23125	277	0	139	0	0	0	0	0	0	780	0	0	0	0	0	23	0	0	0	0	0	0	614	0	0
CF817-3A	10.75	97431	97450	0	0	0	0	451	17	0	39	0	11251	0	16935	0	54772	0	11	0	0	0	0	0	0	0	0	31	0	0	13840	0	0
CF817-3A	13.25	1657	1657	0	0	0	0	718	85	0	0	0	0	0	520	0	190	122	0	0	0	0	0	0	0	0	0	0	0	0	0	22	0
CF817-3A	15.75	1686	1686	0	0	0	0	165	0	0	18	0	0	473	76	0	954	0	0	0	0	0	0	0	0	0	0	0	0	0	0	0	0
CF817-3A	18.25	12078	12154	0	0	0	0	4075	4461	0	21	0	0	0	12	0	3492	0	0	0	0	0	0	17	0	0	0	0	0	0	0	0	0
CF817-3A	20.75	13529	13529	0	0	0	0	10225	691	0	34	0	0	0	13	0	2012	361	0	0	0	0	0	43	0	0	0	0	0	0	130	0	0
CF817-3A	25.75	8437	8437	0	0	0	0	8437	0	0	0	0	0	0	0	0	0	0	0	0	0	0	0	0	0	0	0	0	0	0	0	0	0
CF817-3A	28.25	107403	116021	0	0	0	0	105788	14	0	102	0	0	0	34	0	1424	0	0	0	0	0	0	0	0	0	0	0	0	0	0	0	0
CF817-3A	30.75	16201	16247	0	0	0	0	0	543	112	11826	0	0	0	149	0	27	0	0	0	0	0	0	0	0	0	22	49	0	0	3399	0	0
CF817-3A	38.25	8242	8242	0	0	0	0	0	15	0	20	0	0	0	0	0	12	0	0	0	0	0	0	0	0	0	0	35	0	0	8115	0	0
CF817-3A	40.75	128168	128239	0	0	0	0	0	128071	0	44	0	0	0	0	0	0	0	0	0	0	0	0	0	0	0	0	0	0	0	0	0	0
CF817-3A	43.25	52085	52085	0	0	0	0	0	0	0	24329	27085	0	0	0	0	27	0	626	0	0	0	0	0	0	0	0	0	0	0	18	0	0
CF817-3A	45.75	1977	1977	0	0	0	0	1953	11	0	13	0	0	0	0	0	0	0	0	0	0	0	0	0	0	0	0	0	0	0	0	0	0
CF817-3A	48.25	23403	32676	0	0	0	0	709	22605	0	36	0	0	0	0	0	0	0	53	0	0	0	0	0	0	0	0	0	0	0	0	0	0
CF817-3A	50.75	3412	3412	0	0	0	0	0	3052	0	123	0	0	0	0	0	68	0	0	0	0	0	0	0	0	0	0	26	0	0	0	22	0
CF817-3A	53.25	70797	79458	0	0	0	0	486	30	0	70264	0	0	0	0	0	17	0	0	0	0	0	0	0	0	0	0	0	0	0	0	0	0
CF817-3A	55.75	43007	43007	0	0	0	0	15561	27401	0	45	0	0	0	0	0	0	0	0	0	0	0	0	0	0	0	0	0	0	0	0	0	0
CF817-3A	58.25	24113	24113	0	0	0	0	0	420	0	23681	0	0	0	0	0	0	0	0	0	0	0	0	0	0	0	0	0	0	0	0	0	0
CF817-3A	63.25	11983	11983	0	0	0	0	8414	3555	0	0	0	0	0	0	0	14	0	0	0	0	0	0	0	0	0	0	0	0	0	0	0	0
CF817-3A	65.75	15671	15671	0	0	0	0	778	14882	0	0	0	0	0	0	0	11	0	0	0	0	0	0	0	0	0	0	0	0	0	0	0	0
CF817-3A	68.25	12300	13659	0	0	0	0	1173	11101	0	0	0	0	0	0	0	26	0	0	0	0	0	0	0	0	0	0	0	0	0	0	0	0
CF817-3A	70.75	62523	62523	0	0	0	0	3554	20242	2271	36411	0	0	0	0	0	14	0	0	0	0	0	0	0	0	0	0	0	0	0	0	0	0
CF817-3A	73.25	57763	57763	0	0	0	0	0	6878	10602	40044	0	0	0	0	0	0	0	0	0	164	0	0	0	0	0	0	0	0	0	0	0	0
CF817-3A	75.75	72231	76446	0	0	0	0	759	57513	9754	3204	0	0	0	0	0	32	0	0	0	0	0	0	0	0	564	0	388	0	0	0	0	0
CF817-3A	78.25	58415	58415	0	0	0	0	0	25812	25627	19	0	0	0	0	0	649	5797	0	0	486	0	0	0	0	0	0	14	0	11	0	0	0
CF817-3A	80.75	104049	107479	0	0	0	0	0	40983	26970	49	0	2323	18618	0	0	1292	9669	0	0	0	0	33	0	216	0	2027	0	0	1858	0	0	0
CF817-3A	83.25	72668	72668	0	0	0	0	0	73	53061	43	0	0	0	14	0	5661	13691	0	0	0	0	0	0	0	0	44	13	0	0	46	0	0
CF817-3A	85.75	18844	18935	0	0	0	0	0	18	16165	0	0	0	0	18	0	181	2462	0	0	0	0	0	0	0	0	0	0	0	0	0	0	0
CF817-3A	88.25	34269	34281	0	0	0	0	0	42	9623	21	0	0	0	8144	2582	3072	8706	29	0	0	0	51	0	0	660	0	518	0	0	15	794	0
CF817-3A	90.75	25023	25038	0	0	0	0	0	17	0	2202	0	0	0	348	8257	3563	1713	0	0	0	0	92	0	0	0	1376	6203	0	0	0	1234	0
CF817-3A	93.25	15430	15430	0	0	0	0	0	112	0	0	0	0	0	4247	0	81	0	0	14	0	0	29	0	537	0	0	7522	0	0	0	0	2820
CF817-3A	95.75	21599	34863	0	0	0	0	0	13	0	0	0	0	0	5714	0	7331	1385	22	0	0	0	0	0	5342	0	396	1375	0	0	0	0	0
CF817-3A	98.25	8133	12590	0	0	0	0	0	0	0	0	0	0	0	0	0	1130	2955	0	0	0	0	0	0	0	0	0	4032	0	0	0	0	0
CF817-3A	100.75	15140	15140	0	0	0	0	0	139	0	39	3814	0	0	0	0	18	0	0	0	0	0	0	0	0	0	0	11003	0	0	0	0	0
CF817-3A	103.25	136900	137021	0	0	0	0	271	121	0	43	2662	0	0	0	0	114226	8670	0	0	1311	0	0	57	0	15	0	9505	0	0	0	0	0
CF817-3A	105.75	248967	248967	0	0	0	0	0	21	0	30	0	0	0	0	0	197050	34245	0	0	0	0	0	0	0	0	0	15333	745	0	0	1524	0
CF817-3A	108.25	30523	30523	0	0	0	0	0	0	0	0	0	0	0	0	0	54	0	0	3372	0	0	0	0	0	0	0	27067	0	0	0	0	0
CF817-3A	110.75	97169	97184	0	0	0	0	0	117	0	120	0	0	0	0	15	33	76961	0	529	0	0	0	0	0	0	0	19323	0	0	0	0	0
19CF8-07C-a	223.5	1915	2054	0	0	0	0	1837	0	0	0	0	0	0	0	0	78	0	0	0	0	0	0	0	0	0	0	0	0	0	0	0	0
19CF8-07C-a	225.5	1717	1793	0	0	0	0	1717	0	0	0	0	0	0	0	0	0	0	0	0	0	0	0	0	0	0	0	0	0	0	0	0	0
19CF8-07C-w	226.5	22928	22928	0	0	0	0	22192	0	0	0	0	0	0	0	0	603	0	87	0	0	0	0	46	0	0	0	0	0	0	0	0	0
19CF8-07C-w	230.5	29634	35798	0	0	0	0	25050	0	0	0	0	0	0	0	0	4584	0	0	0	0	0	0	0	0	0	0	0	0	0	0	0	0
19CF8-07C-a	233.5	1450	1450	0	0	0	0	356	74	0	0	1020	0	0	0	0	0	0	0	0	0	0	0	0	0	0	0	0	0	0	0	0	0
19CF8-07C-a	235.5	3088	3088	0	0	0	0	3088	0	0	0	0	0	0	0	0	0	0	0	0	0	0	0	0	0	0	0	0	0	0	0	0	0
19CF8-07C-a	238.5	2045	2045	67	13	0	0	1394	0	0	505	0	0	0	0	0	0	0	0	0	0	0	0	0	0	0	0	0	0	0	0	0	0
19CF8-07C-a	239.5	1534	1683	0	0	56	0	858	0	0	620	0	0	0	0	0	0	0	0	0	0	0	0	0	0	0	0	0	0	0	0	0	0
19CF8-07C-b	240.5	15373	15383	0	0	0	0	9661	4257	1455	0	0	0	0	0	0	0	0	0	0	0	0	0	0	0	0	0	0	0	0	0	0	0
19CF8-07C-a	241.5	2268	2328	0	675	0	0	266	1327	0	0	0	0	0	0	0	0	0	0	0	0	0	0	0	0	0	0	0	0	0	0	0	0
19CF8-07C-b	242.5	7484	10062	1017	0	0	0	6178	276	0	0	0	0	0	0	0	0	0	0	0	0	0	0	0	0	0	0	0	0	0	0	0	0
19CF8-07C-a	243.5	3185	3185	0	0	0	0	1880	949	0	356	0	0	0	0	0	0	0	0	0	0	0	0	0	0	0	0	0	0	0	0	0	0
19CF8-07C-b	244.5	11503	11503	0	0	0	0	5756	3304	2443	0	0	0	0	0	0	0	0	0	0	0	0	0	0	0	0	0	0	0	0	0	0	0
19CF8-07C-a	245.5	3728	4686	0	0	711	0	2301	716	0	0	0	0	0	0	0	0	0	0	0	0	0	0	0	0	0	0	0	0	0	0	0	0
19CF8-07C-b	246.5	10917	11750	886	0	0	0	6970	845	2216	0	0	0	0	0	0	0	0	0	0	0	0	0	0	0	0	0	0	0	0	0	0	0
19CF8-07C-a	247.5	3277	6096	0	2826	0	0	0	127	300	0	0	0	0	0	0	0	0	0	0	0	0	0	0	0	0	0	0	0	0	0	0	0
19CF8-07C-b	248.5	13703	15724	0	0	0	0	9427	4157	119	0	0	0	0	0	0	0	0	0	0	0	0	0	0	0	0	0	0	0	0	0	0	0
19CF8-07C-a	249.5	5712	5712	95	0	0	0	1912	2048	1420	0	0	0	0	0	0	0	0	237	0	0	0	0	0	0	0	0	0	0	0	0	0	0
19CF8-07C-a	250.5	11505	11505	0	0	0	0	9646	27	1707	125	0	0	0	0	0	0	0	0	0	0	0	0	0	0	0	0	0	0	0	0	0	0
19CF8-07C-a	251.5	5148	5148	0	0	0	0	2106	0	0	3042	0	0	0	0	0	0	0	0	0	0	0	0	0	0	0	0	0	0	0	0	0	0
19CF8-07C-b	252.5	15664	19573	0	0	0	0	12441	1779	0	1414	0	0	0	0	0	0	0	0	0	0	0	0	0	0	0	0	0	0	0	0	0	0
19CF8-07C-a	253.5	1920	1920	27	0	0	0	1735	158	0	0	0	0	0	0	0	0	0	0	0	0	0	0	0	0	0	0	0	0	0	0	0	0
19CF8-07C-w	254.5	5602	6313	0	0	0	0	5003	0	599	0	0	0	0	0	0	0	0	0	0	0	0	0	0	0	0	0	0	0	0	0	0	0
19CF8-07C-a	255.5	9428	9428	0	0	0	0	6377	187	0	2864	0	0	0	0	0	0	0	0	0	0	0	0	0	0	0	0	0	0	0	0	0	0
19CF8-07C-a	257.5	2257	3978	0	0	0	0	0	0	0	2257	0	0	0	0	0	0	0	0	0	0	0	0	0	0	0	0	0	0	0	0	0	0
19CF8-07C-a	258.5	10082	10082	0	0	0	0	0	693	0	8961	0	0	0	0	0	0	0	0	0	370	0	0	0	0	0	0	0	0	0	0	0	0
19CF8-07C-a	259.5	13003	13003	0	0	0	0	380	119	0	12478	0	11	0	0	0	0	0	0	0	0	0	0	0	0	0	0	0	0	0	0	0	0
19CF8-07C-a	261.5	6910	6910	0	0	0	0	311	2607	0	12	0	0	0	0	0	0	0	0	0	0	3980	0	0	0	0	0	0	0	0	0	0	0
19CF8-07C-w	262.5	5176	5176	0	0	0	0	0	0	0	5176	0	0	0	0	0	0	0	0	0	0	0	0	0	0	0	0	0	0	0	0	0	0
19CF8-07C-a	263.5	10879	12392	0	0	0	0	566	2418	0	0	0	7895	0	0	0	0	0	0	0	0	0	0	0	0	0	0	0	0	0	0	0	0
19CF8-07C-a	265.5	3592	3592	0	0	0	579	0	2758	184	51	0	0	0	0	0	0	0	0	0	0	0	0	0	0	0	0	0	0	0	0	0	0
19CF8-07C-a	267.5	5482	6439	0	0	0	3925	0	0	0	0	0	0	0	0	0	265	1256	0	0	0	0	0	0	0	0	0	0	0	0	0	0	0
19CF8-07C-a	268.5	7326	7832	0	0	0	6586	0	0	638	0	0	0	0	0	0	0	102	0	0	0	0	0	0	0	0	0	0	0	0	0	0	0
19CF8-07C-w	268.5	14846	14846	0	0	0	9477	0	0	5369	0	0	0	0	0	0	0	0	0	0	0	0	0	0	0	0	0	0	0	0	0	0	0
19CF8-07C-w	270.5	2775	2775	0	0	0	0	0	0	0	0	0	0	0	0	0	0	2775	0	0	0	0	0	0	0	0	0	0	0	0	0	0	0
19CF8-07C-w	272.5	3084	6158	0	0	0	0	0	0	0	0	0	0	0	0	0	0	0	0	0	0	0	0	0	3084	0	0	0	0	0	0	0	0

[a]Designations “-a”, “-w”, and “-b” refer to archive half, working half, and both (combined data from replicate depths), respectively.
[b]Reads below the minimum read threshold were assigned “0” for all taxa.

Table S4. Extraction control data for Lake CF8 cores

Core	ID	Post-filter reads	Pre-filter reads	Rhododendron	Salicaceae	Vaccinium uliginosum	Empetrum	Bistorta vivipara	Poaceae	Poa	Luzula	Oxyria digyna
CF817-3A	extr_ctrl_A	1	0	0	0	0	0	0	0	1	0	0
CF817-3A	extr_ctrl_B	0	0	0	0	0	0	0	0	0	0	0
CF817-3A	extr_ctrl_C	0	0	0	0	0	0	0	0	0	0	0
CF817-3A	extr_ctrl_D	1	0	0	0	0	0	1	0	0	0	0
CF817-3A	extr_ctrl_E	0	0	0	0	0	0	0	0	0	0	0
19CF8-07C-w	extr_ctrl_2019_3	21	21	0	0	0	0	0	0	0	0	21
19CF8-07C-w	extr_ctrl_2019_4	11	0	0	8	3	0	0	0	0	0	0
19CF8-07C-w	extr_ctrl_2019_5	3	17	0	0	0	0	0	3	0	0	0
19CF8-07C-a	extr_ctrl_2020_1	26	26	0	26	0	0	0	0	0	0	0
19CF8-07C-a	extr_ctrl_2020_2	40	2461	0	0	4	36	0	0	0	0	0
19CF8-07C-a	extr_ctrl_2020_3	27	20	5	20	0	0	0	2	0	0	0
19CF8-07C-a	extr_ctrl_2020_4	10	0	0	9	0	0	0	0	0	1	0

Table S5. Pollen data for Lake CF8 cores

Core	Com-posite depth (cm)	Age (cal yr BP)	Unit	Boreal trees (%)	Alnus (%)	Betula (%)	Salix (%)	Ericaceae (%)	Cyper-aceae (%)	Poaceae (%)	Rosaceae (%)	Caryo-phyllaceae (%)	Oxyria digyna (%)	Saxifra-gaceae (%)	Pollen sum (grains)	Pollen concen-tration (grains/cc)	Pollen concen-tration (grains/g)	July T min (ºC)	July T best (ºC)	July T max (ºC)
2002-CF8	5	869	Holocene	1.26	1.26	2.32	6.74	54.74	12.42	6.32	0.42	3.58	7.37	0.42	475	3068	11802	4.3	4.8	5.0
2002-CF8	13	1543	Holocene	0.60	0.00	1.00	11.38	55.09	15.37	7.98	0.00	1.80	4.99	0.40	501	7354	29416	5.0	5.0	5.0
2002-CF8	23	2556	Holocene	1.26	0.25	2.77	8.06	48.11	18.64	8.31	0.00	1.76	5.29	1.51	397	4491	14970	4.5	4.8	5.0
2002-CF8	32	3582	Holocene	0.44	2.83	1.74	9.37	32.24	27.45	9.15	0.00	1.09	11.11	0.44	459	3949	14626	5.0	5.2	5.6
2002-CF8	40	4548	Holocene	1.02	3.30	2.54	11.17	23.86	32.49	5.08	0.00	0.51	16.75	0.51	394	5538	19780	4.0	5.1	6.0
2002-CF8	48	5533	Holocene	0.39	3.13	2.15	10.76	23.68	37.77	5.87	0.00	1.57	11.15	0.59	511	5709	19686	4.0	5.0	6.0
2002-CF8	56	6507	Holocene	0.81	1.62	1.62	13.13	24.04	33.13	6.87	0.00	2.42	13.54	0.81	495	9144	33866	4.0	5.0	6.0
2002-CF8	65	7535	Holocene	0.00	0.77	1.54	8.64	31.09	27.06	13.63	0.00	3.26	9.98	1.73	521	8140	29073	5.0	5.0	5.0
2002-CF8	78	8662	Holocene	0.00	0.22	0.44	5.24	10.92	23.80	25.33	0.44	9.39	21.83	0.66	458	9198	27052	3.0	4.0	5.0
2002-CF8	89	9520	Holocene	0.00	0.00	0.85	0.21	9.94	21.56	15.86	0.21	12.68	29.18	0.85	473	6606	20642	n/a	n/a	n/a
2002-CF8	105	10610	Holocene	0.28	0.28	3.12	0.00	0.57	10.48	25.21	0.00	2.27	44.76	2.55	353	3997	13322	n/a	n/a	n/a
2002-CF8	121	11515	Holocene	2.04	2.04	17.35	11.22	14.29	22.45	8.16	0.00	1.02	16.33	1.02	98	603	685	n/a	n/a	n/a
2004-CF8	204	n/a	LIG	0.74	0.93	11.92	16.01	36.50	23.65	5.59	0.00	1.86	0.19	1.49	537	46631	40269	4.0	5.2	7.7
2004-CF8	209	n/a	LIG	0.58	1.54	11.18	11.37	39.11	22.93	8.67	0.00	1.73	0.58	0.58	519	67920	75132	4.0	5.3	7.9
2004-CF8	214	n/a	LIG	0.91	0.91	15.06	9.26	39.75	22.87	5.26	0.18	2.90	0.36	0.91	551	51713	102200	4.0	5.2	7.6
2004-CF8	219	n/a	LIG	0.37	0.18	9.98	12.57	48.43	17.93	4.99	0.00	1.29	0.00	1.48	541	71470	148014	4.0	5.8	8.0
2004-CF8	226	n/a	LIG	1.16	1.93	8.70	15.67	30.17	29.21	5.03	0.19	4.06	0.97	1.74	517	38740	75960	4.5	4.8	5.0
2004-CF8	235	n/a	LIG	1.69	3.75	25.89	13.32	15.38	26.64	7.69	0.19	0.56	0.56	1.69	533	17176	44041	6.0	7.3	9.0
2004-CF8	239	n/a	LIG	2.10	9.63	34.68	9.46	12.78	20.67	6.13	0.00	1.23	0.35	0.88	571	21026	60073	6.0	7.3	9.0
2004-CF8	247	n/a	LIG	1.07	10.00	53.57	4.82	8.04	17.14	2.50	0.00	0.36	0.00	0.54	560	36217	90544	6.0	7.6	10.7
2004-CF8	252	n/a	LIG	0.18	11.21	54.78	6.99	5.33	18.57	1.65	0.00	0.18	0.00	0.37	544	44338	96388	7.0	8.0	9.9
2004-CF8	257	n/a	LIG	0.35	6.08	54.17	7.47	7.47	19.10	2.60	0.52	0.17	0.00	0.35	576	35056	54775	6.0	7.7	11.0
2005-CF8	263.5	n/a	LIG	0.00	4.95	25.46	5.86	6.96	15.93	10.99	8.06	3.11	8.79	1.83	546	9572	11533	4.0	8.2	13.0

SI References

1. Kerwin MW, Overpeck JT, Webb RS, Anderson KH (2004) Pollen-based summer temperature reconstructions for the eastern Canadian boreal forest, subarctic, and Arctic. *Quaternary Science Reviews* 23:1901–1924.
2. Polunin N (1951) The Real Arctic: Suggestions for its Delimitation, Subdivision and Characterization. *Journal of Ecology* 39(2):308–315.
3. Team C (2003) *Circumpolar Arctic Vegetation Map*.
4. Miller GH, Andrews JT, Short SK (1977) The last interglacial-glacial cycle, Clyde foreland, Baffin Island, N.W.T.: Stratigraphy, biostratigraphy, and chronology. *Canadian Journal of Earth Sciences* 14:2824–2857.
5. Blaauw M, Christen JA (2011) Flexible paleoclimate age-depth models using an autoregressive gamma process. *Bayesian Analysis* 6(3):457–474.
6. Wickham H (2016) ggplot2: Elegant Graphics for Data Analysis.
7. Bennett KD (1996) Determination of the number of zones in a biostratigraphical sequence. *New Phytologist* 132(1):155–170.
8. Juggins S (2017) rioja: Analysis of Quaternary Science Data, R package version 0.9-21. Available at: http://cran.r-project.org/package=rioja.
9. Oksanen J, et al. (2016) vegan: Community Ecology Package. Available at: http://cran.r-project.org/package=vegan.
10. McFarlin JM, et al. (2018) Pronounced summer warming in northwest Greenland during the Holocene and Last Interglacial. *Proceedings of the National Academy of Sciences of the United States of America*:201720420.
11. Landais A, et al. (2016) How warm was Greenland during the last interglacial period? *Climate of the Past* 12:1933–1948.
12. Yau AM, Bender ML, Robinson A, Brook EJ (2016) Reconstructing the last interglacial at Summit, Greenland: Insights from GISP2. *Proceedings of the National Academy of Sciences of the United States of America* 113(35):9710–5.
13. Members NGICP (2004) High-resolution record of Northern Hemisphere climate extending into the last interglacial period. *Nature* 431:147–151.
14. Axford Y, et al. (2011) Chironomids record terrestrial temperature changes throughout Arctic interglacials of the past 200,000 yr. *Geological Society of America Bulletin* 123(7–8):1275–1287.
15. Francis DR, Wolfe AP, Walker IR, Miller GH (2006) Interglacial and Holocene temperature reconstructions based on midge remains in sediments of two lakes from Baffin Island, Nunavut, Arctic Canada. *Palaeogeography, Palaeoclimatology, Palaeoecology* 236(1–2):107–124.
16. Fréchette B, Wolfe AP, Miller GH, Richard PJH, de Vernal A (2006) Vegetation and climate of the last interglacial on Baffin Island, Arctic Canada. *Palaeogeography, Palaeoclimatology, Palaeoecology* 236(1–2):91–106.
17. Miller GH, et al. (1999) Stratified interglacial lacustrine sediments from Baffin Island, Arctic Canada: chronology and paleoenvironmental implications. *Quaternary Science Reviews* 18(6):789–810.
18. Members C-LIP (2006) Last Interglacial Arctic warmth confirms polar amplification of climate change. *Quaternary Science Reviews* 25:1383–1400.
19. Morgan A V, Kuc M, Andrews JT (1993) Paleoecology And Age Of The Flitaway And Isortoq Interglacial Deposits, North-Central Baffin-Island, Northwest-Territories, Canada. *Canadian Journal of Earth Sciences* 30(5):954–974.
20. Stuiver M, Reimer PJ, Reimer RW (2020) CALIB 8.2 [WWW program] at http://calib.org, accessed 2020-12-13.
21. Reimer PJ, et al. (2020) The IntCal20 Northern Hemisphere Radiocarbon Age Calibration Curve (0-55 cal kBP). *Radiocarbon* 62(4):725–757.